Economic Geology

BULLETIN OF THE SOCIETY OF ECONOMIC GEOLOGISTS

VOL. 104 March–April 2009 NO. 2

Iron Skarns of the Vegas Peladas District, Mendoza, Argentina*

JOSEFINA M. PONS,† MARTA FRANCHINI,

CONICET, Centro Patagónico de Estudios Metalogenéticos-CIMAR, Facultad de Ingeniería, Universidad Nacional del Comahue, Buenos Aires 1400 (8300) Neuquén, Patagonia, Argentina

LAWRENCE MEINERT,

Department of Geosciences, Smith College, Northampton, Massachusetts 01063

CLEMENTE RECIO,

Servicio General de Isótopos Estables, Facultad de Ciencias Universidad de Salamanca, Plaza de los caídos s/n (37008), Spain

AND RICARDO ETCHEVERRY,

CONICET, Centro Patagónico de Estudios Metalogenéticos-CIMAR, Facultad de Ingeniería, Universidad Nacional del Comahue, Buenos Aires 1400 (8300) Neuquén, Patagonia, Argentina, and

INREMI, Facultad de Ciencias Naturales y Museo, Universidad Nacional de La Plata, Calle 64 n°3 (1900) La Plata, Argentina

Abstract

The Andean belt southwest of Mendoza, Argentina, hosts 23 Fe, Fe-Cu, and Cu (Ag) deposits classified variously in the literature as skarn, iron oxide-copper-gold (IOCG), and manto-type Cu deposits. The Vegas Peladas deposit is one of the best exposed Fe skarns with mineral assemblages and hydrothermal features similar to many other calcic Fe skarns of the world. The plutonic rocks of Vegas Peladas consist of a series of diorite to granite stocks, dikes, and sills. The major-, trace-, and rare earth-element geochemistry analyses of these igneous rocks indicate they were derived from subarc mantle sources. The Vegas Peladas deposit formed by the overprinting of two different metamorphic and metasomatic events associated with early diorite and later granite intrusions.

Alteration associated with the early diorite intrusions consists of a metamorphic halo (800 m wide) and a zoned calcic skarn with inner garnet ($Ad_{31-89}\,Py_{0-2}$) + clinopyroxene + magnetite + quartz, intermediate garnet ($Ad_{38-51}\,Py_{1-2}$) ± clinopyroxene, and distal veins of garnet (Ad_{96-100}) ± pyroxene ($Hd_{72-29}\,Jo_{1-4}$). The latest alteration consists of widespread albite (Ab_{96-98}) ± epidote ± quartz ± calcite ± chlorite ± pyrite ± titanite. Magnetite and hematite are the main iron ore minerals and occur as massive orebodies and veins associated with retrograde epidote and amphibole. Alteration of the diorite consists of early orthoclase + quartz followed by later amphibole ± quartz ± magnetite ± epidote ± feldspar.

The granite-related skarn overprints the earlier diorite-related skarn and consists of garnet + clinopyroxene + scapolite (Me_{28-36}) ± quartz ± alkali feldspar endoskarn and a zoned exoskarn with proximal garnet ± clinopyroxene ± quartz, intermediate green garnet ($Ad_{30-81}\,Py_{0-1}$) + clinopyroxene ($Di_{82-93}\,Jo_{4-2}$), and distal scapolite (Me_{25-36}) ± ferroactinolite ± pyrite veins.

Based on fluid inclusion, stable isotope, and REE data, the prograde skarn formed at depths of ~ 3.5 km under lithostatic pressure of ~1 kbar, from high temperature (670°–400°C), saline and iron-rich (>50 wt % NaCl equiv, NaCl ± KCl ± $FeCl_2$) magmatic fluids (garnet $\delta^{18}O_{H2O}$ = 7.2–8.5‰) with intermediate oxygen fugacity. Iron ore and retrograde exoskarn assemblages formed under hydrostatic condition after the fracturing of early skarn. Fluids in this stage had lower temperature (T<320°C) and salinity (<48.5 wt % NaCl equiv, NaCl-KCl-$FeCl_n$-H_2O-$CO_3^=$). The mineralogy and positive Eu anomaly of the retrograde assemblage indicate an environment with high oxygen fugacity. Mixing and dilution of early magmatic fluids with external fluids (e.g., meteoric waters) caused a decrease in fluid temperature, salinity, and total REE concentration in latest stage of the skarn formation (epidote, quartz, and calcite $\delta^{18}O_{H2O}$ = –4.66 to +4.3‰; $\delta^{13}C_{fluid}$ = –10.3 to –7.2‰). The intrusion of the granite pluton increased the wall-rock temperature (>550°C) and also generated saline (30.3 to 45.3 wt % NaCl equiv, H_2O-NaCl-$FeCl_2$) + vapor fluids by immiscibility that redistributed some of the iron from the previous skarn.

† Corresponding author: e-mail, jpons@uncoma.edu.ar

*A digital supplement to this paper is available at <http://www.geoscience world.org/> or, for members' access and for subscribers, on the SEG website, <http://www.segweb.org>

Introduction

Vegas Peladas is one of 23 Fe, Fe-Cu and Cu (Ag) prospects in a 20- by 200-km zone along the Andean belt of southwest Mendoza province, Argentina (34°–36°S and 69.5°–70°W: Figs. 1 and 2; Franchini et al., 2007). The deposits share a number of mineralogical characteristics although individual deposits have been classified as skarn (as described by Einaudi et al., 1981; Meinert et al., 2005), iron oxide-copper-gold-(IOCG) type systems (as described by Williams, 1999; Pollard, 2000), and manto-type Cu deposits (as described by Espinoza et al., 1996) (see Franchini et al., 2007). This article describes the geology of the Vegas Peladas deposit and its alteration characteristics and documents a variety of skarn types among the prospects in the Mendoza belt. The excellent outcrops of the Vegas Peladas Fe skarns make this an ideal region to shed light on the genetic model for this type of deposit.

Vegas Peladas (35°20'07"S, 69°57'28"W) is located 35 km northwest of Malargüe, Argentina, in the Vegas Peladas glacial valley on the northeast slope of Las Minas Hill at an elevation of 2,900 m (Fig. 2). The district was first studied by Angelelli (1942) and more recently by Arrospide (1972), who described the geologic setting and proposed a metasomatic origin for the iron ore. The present study is the result of three months of surface mapping between 2002 and 2004 and subsequent petrographic and analytical work.

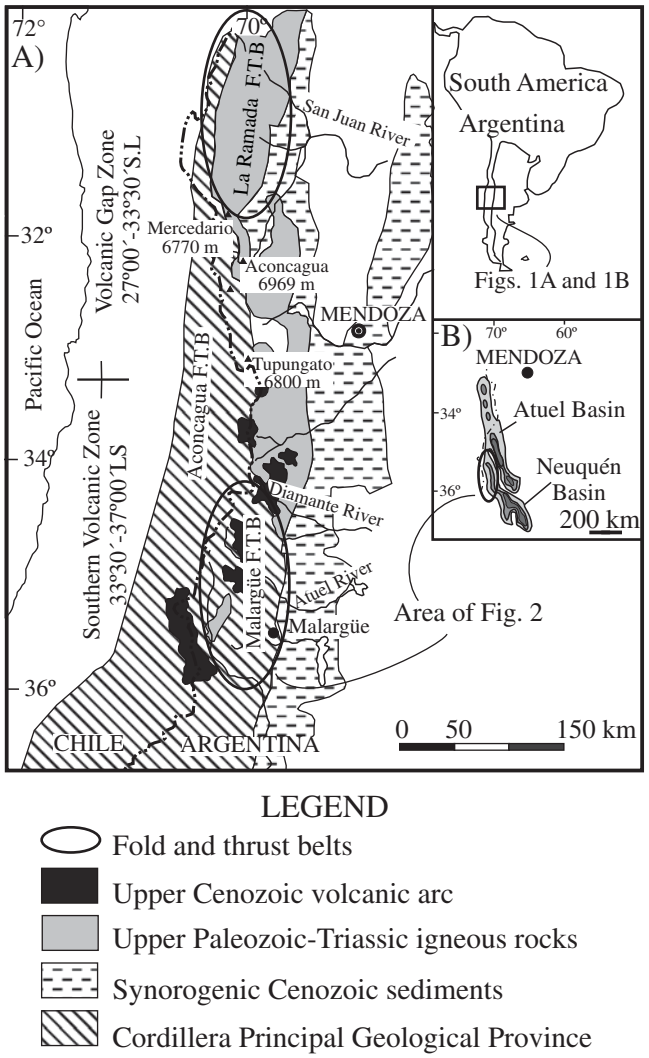

LEGEND

- Fold and thrust belts
- Upper Cenozoic volcanic arc
- Upper Paleozoic-Triassic igneous rocks
- Synorogenic Cenozoic sediments
- Cordillera Principal Geological Province

Fig. 1. Location map of (A) the Malargüe fault and thrust belt in the Southern volcanic zone of the Andes Cordillera and (B) the Neuquén basin in the Cordillera Principal of the southwest Mendoza province, Argentina.

Regional Geology

Vegas Peladas is located in the continental margin of South America, 317 km east of the trench where the oceanic Nazca plate subducts eastward beneath the continental plate. Vegas Peladas is in the Andes mountain segment known as Cordillera Principal of southwest Mendoza (Mpodozis and Ramos, 1989; Ramos and Nullo, 1993; Ramos, 1999a) (Fig. 2A, B). The Paleozoic basement was formed from multistage accretion events that started in the Neoproterozoic (Mpodozis and Ramos, 1989; Ramos, 1999a, b) and culminated with the extensional collapse of the orogenic belt during the late Paleozoic to early Mesozoic. This extensional event was responsible for the initial configuration of the Neuquén basin (Borrello, 1969; Vicente, 1975; Uliana et al., 1989). The basin was later filled with more than 6,000 m of Mesozoic and Tertiary sedimentary rocks in the southwest Mendoza area (Yrigoyen, 1979) deposited during several sedimentary, marine, and continental cycles represented by siliciclastic, calcareous, and evaporitic layers (Legarreta et al., 1993). The stratigraphic section is illustrated in Figure 2C.

The current structural setting is the consequence of normal subduction of the Nazca slab underneath the American plate, which began in the Tertiary (Gulisano and Gutiérrez Pleimling, 1995) and formed the thick-skinned Malargüe fold and thrust belt (Ramos et al., 1996). This belt consists of thrust slices of the sedimentary sequences with eastern vergence and north-south, northeast-southwest, and northwest-southeast trends (Fig. 2B). A period of intense magmatism consisting of three magmatic cycles was synchronous with the compression events (Ramos and Nullo, 1993): an upper Eocene to lower Oligocene event restricted to the southwest Mendoza region, a Miocene event consisting of widespread intrusive and volcanic rocks (Bouza, 1991; Baldauf et al., 1992; Ramos and Nullo, 1993), and a Pliocene to Quaternary event (Fig. 2B), which formed the Transitional southern volcanic zone (TSVZ) (López-Escobar, 1984). The plutonic rocks of the Vegas Peladas are part of the Miocene magmatic cycle and consist of a series of diorite to granite stocks, dikes, and sills.

Local Geology

The oldest geologic units in the Vegas Peladas district are the early to middle Jurassic marine sedimentary rocks of the Puchenque (Hettangian-lower Callovian) and Calabozo (early-middle Callovian) formations. These units crop out to the northeast of Las Minas Hill on both sides of the Vegas Peladas Creek (Fig. 3A, B). The Puchenque Formation consists of 450 m of claystone with interbedded siltstone, black shale, and sandstone with calcareous cement. The Calabozo Formation is a 50- to 100-m-thick homogeneous package of mudstone-wackestone. Evaporitic rocks of the Auquilco Formation (late Oxfordian to Kimmeridgian Lotena-Chacay Group) crop out discontinuously along the northeast side of Vegas Peladas Creek and overlay the previous units with a tectonic contact (Fig. 3A). Southeast of

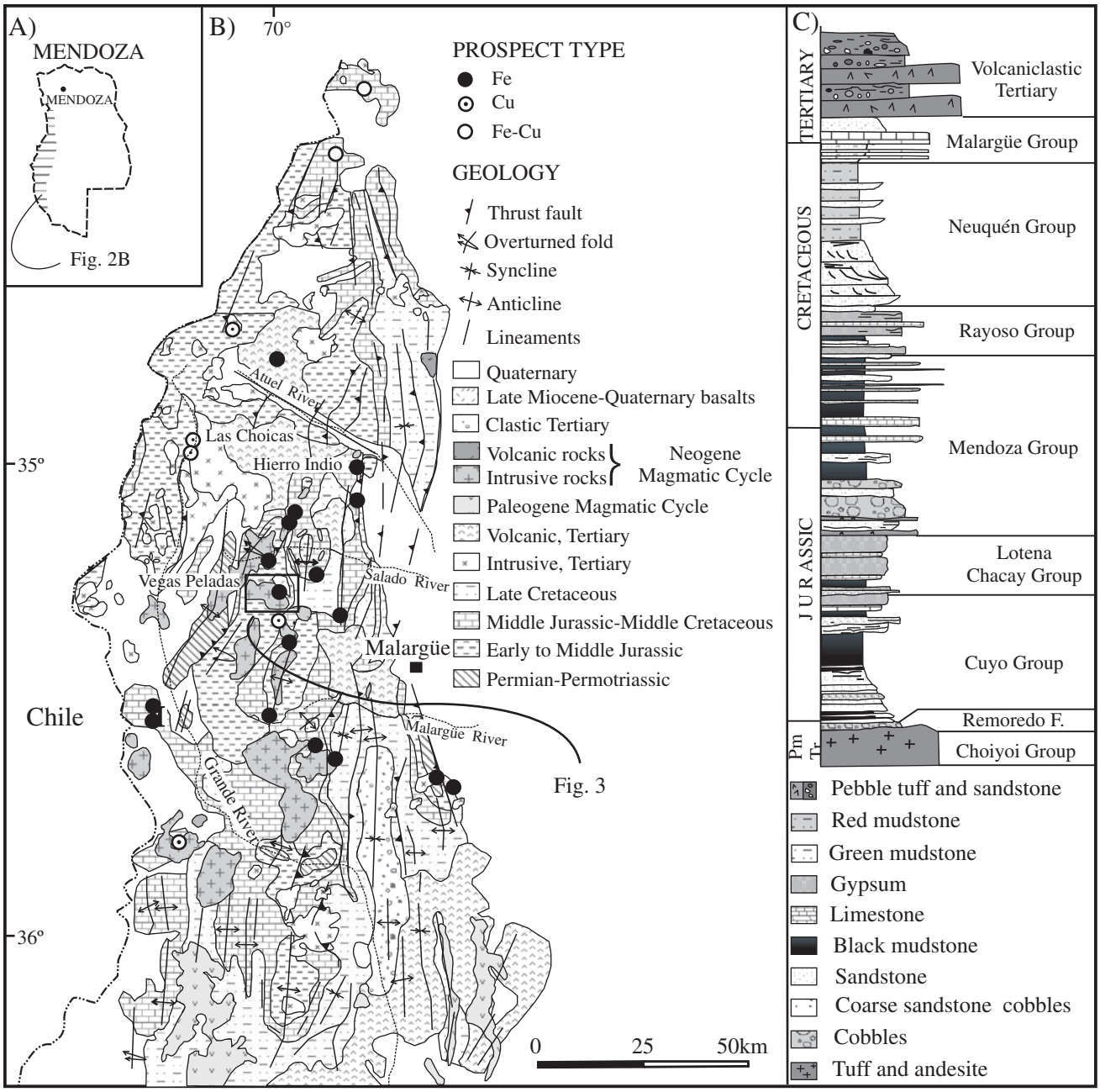

FIG. 2. A. Inset showing the location of Figure 2B. B. Geologic map of the thrust belt of Malargüe (modified from Kozlowski et al., 1993; Mendez et al., 1995; Nullo et al., 2002) showing the location of the Vegas Peladas iron skarns and other Fe, Fe-Cu, and Cu (Ag) prospects (after Franchini and Dawson, 1999; Franchini et al., 2007). C. Detail of the stratigraphic column (modified from Legarreta et al., 1993) in the thrust belt of Malargüe. F. = formation, Pm = Permian, Tr = Triassic.

Vegas Peladas Creek, continental and clastic sedimentary rocks of the Tordillo Formation (Mendoza Group) unconformably overlie the Auquilco Formation (Fig. 3A).

On both sides of the Vegas Peladas Creek, the sedimentary rocks were intruded by a series of Neogene plutons, dikes, and sills. In the southeast area of the valley, Quaternary basalts overlie the sedimentary sequence and the intrusive units in angular disconformity. Sediments of glacial, mass-wasting, and fluvial origin partially cover the cirques, slopes, creeks, and valleys (Fig. 3A, B).

At Vegas Peladas, Tertiary compression deformed the Jurassic sedimentary rocks of the Puchenque and Calabozo Formations into a south-southeast–trending anticline that was intruded by a granitic pluton (Fig. 3A, B). The evaporitic rocks of the Aquilco Formation behaved as bedding-plane thrusts with eastern vergence that caused repetition of the Tordillo Formation in the southeast portion of the area. A subvertical fault developed along the anticline axis, cutting the igneous bodies and exposing the contact between the geologic units.

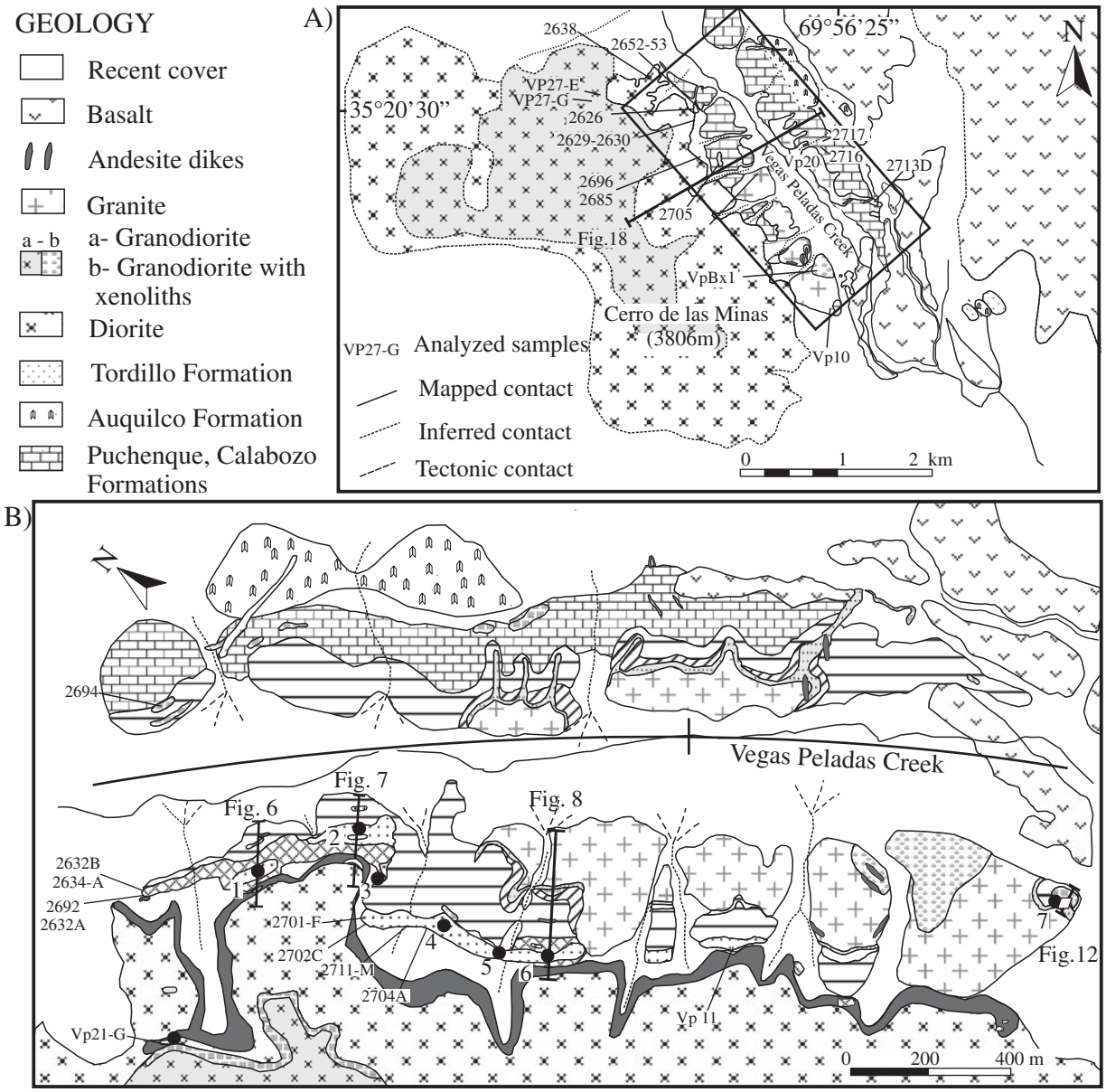

ALTERATION-MINERALIZATION

2711-M Analyzed samples

Cross sections of Figs. 6 to 8 and 12

Fe skarn associated with granite

Iron ore

Exoskarn

Hydrothermal alteration and endoskarn

Hornfels

Hydrothermal alteration in granodiorite

Fe skarn associated with diorite

Massive iron ore

Retrograde alteration

Exoskarn

Hydrothermal alteration and endoskarn

Hornfels

FIG. 3. A. Geologic map of the Vegas Peladas district with the location of analyzed igneous rocks shown in Tables 1, 2, and 5 and the cross section of Figure 18; the box indicates the area of detailed mapping and sampling shown in (B) (modified from Arrospide, 1972; Dessanti, 1978). B. Map of the investigated area showing geology, alteration, mineralization, and location of the cross sections shown in Figures 6, 7, 8, and 12, and the analyzed ore samples, for which results are presented in Tables 2, 3, and 5.

Igneous rocks

Four hypabyssal igneous units have been identified and mapped (Fig. 3A, B): diorite and granodiorite plutons that form the Cerro de las Minas Hill, a granite pluton emplaced in the periphery of the hill and elongated along Vegas Peladas Creek, and andesite dikes and sills that cut the earlier intrusions. The dioritic pluton is the oldest igneous unit. Its composition ranges from diorite to tonalite, with diorite being the most widespread. The diorite and tonalite contain zoned plagioclase, pyroxene, amphibole, biotite, and quartz, with accessory magnetite, minor titanite, and apatite, and traces of zircon. In some diorite samples, amphibole contains relict orthopyroxene and clinopyroxene cores. The texture varies from microporphyritic to glomerophyritic. The granodiorite pluton intruded the northern and central parts of the diorite pluton. It contains plagioclase, amphibole, quartz, and biotite, with accessory magnetite, apatite, and zircon, and its texture varies from granular in the center to porphyritic at the margin.

Locally, the presence of abundant diorite-tonalite xenoliths (50 vol %) within the granodiorite pluton (Fig. 3A, B) and textural evidence for plastic flow suggest that mingling occurred between the diorite-tonalite and granodiorite magmas (Pons et al., 2007). The presence of primary magnetite and biotite in both plutons suggests intermediate oxygen fugacity during their emplacement. The granite pluton intrudes the diorite-tonalite and the granodiorite stocks with sharp contacts in the southeastern part of the district. In the northeastern sector, the contact of the granite with the Puchenque Formation is concordant and characterized by hydraulic fracturing of the sedimentary rock; some fractures are filled with dikes and sills of rhyolite. Andesite dikes and sills intruded all these igneous units and are more abundant at the southeast end of the valley. Rb-Sr isotope analyses of whole rock and biotite yielded an isochron age of 15.19 ± 0.24 Ma for granodiorite (Fig. 3A, sample VP27-E: Pons, 2007).

The chemical classification of these rocks (Fig. 4A; Table 1) is consistent with their mineralogy and similar to other

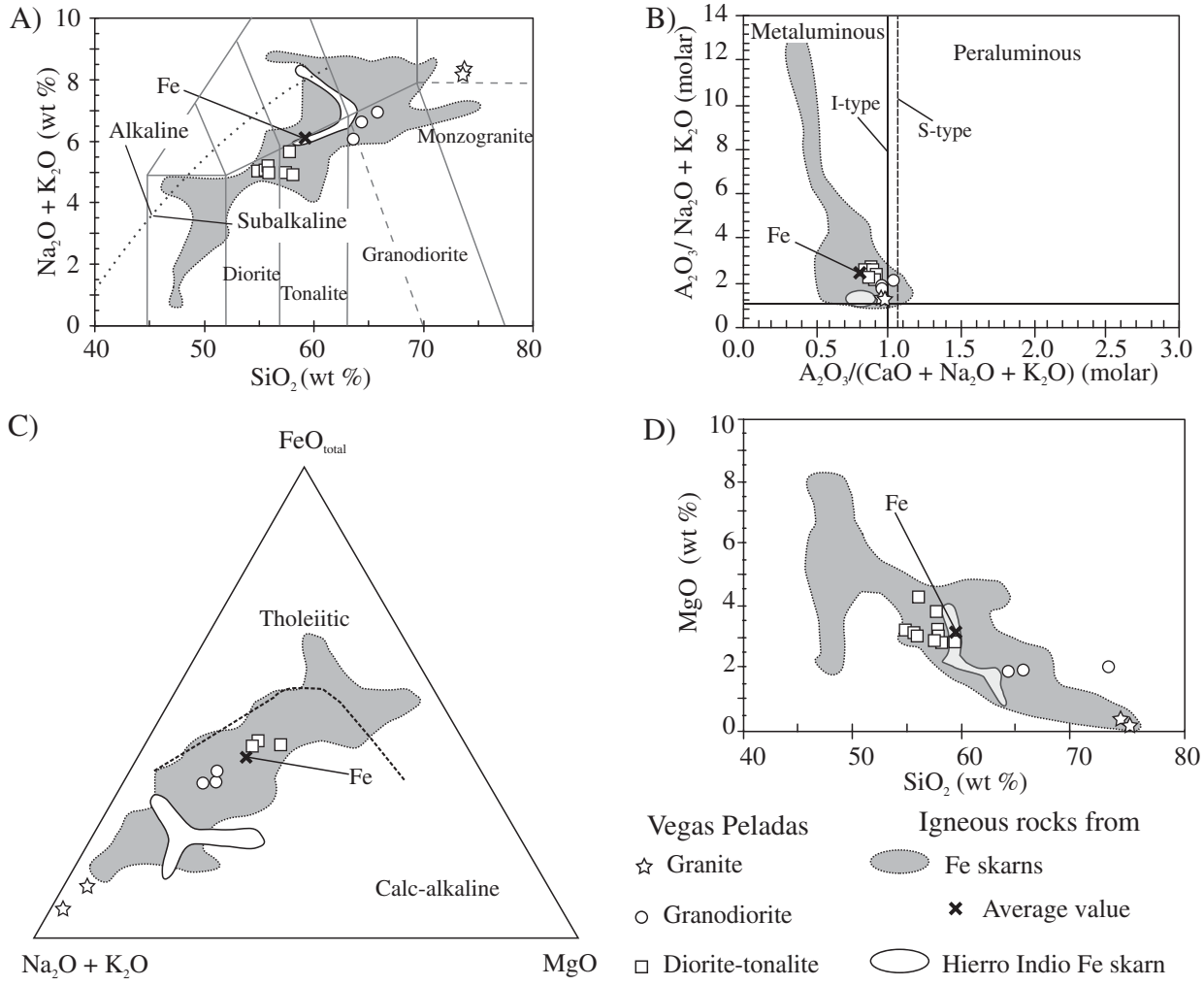

FIG. 4. Chemical characterization of least-altered igneous rocks of Vegas Peladas associated with Fe skarns. The composition of igneous rocks associated with the Hierro Indio Fe skarn (from southwest Mendoza; after Franchini et al., 2005), and with Fe skarns worldwide (from Meinert, 1995) are shown for comparison. A. Total alkalis vs. silica classification (Bellieni et al., 1996). B. Aluminum saturation index. C. AFM diagram with calc-alkali-tholeiitic boundary line from Irvine and Baragar (1971). D. MgO vs. SiO_2 diagram.

TABLE 1. Whole-Rock Major and Trace Element Compositions of Representative Diorite, Granodiorite, Granite, and Rhyolite Samples from Vegas PeladasDistrict

Sample no.	2629	2652	2653	2628	2696	2626	2630	2638	2686	VP21 G	2705	VP27-E1	VP27-G	2713-D	VP10	VP20	VP16
Igneous rocks	Diorite pluton	Diorite pluton	Diorite pluton	Diorite pluton	Diorite pluton	Diorite pluton	Diorite pluton	Diorite pluton	Diorite pluton	Diorite pluton	Granodi-orite dike	Grano-diorite pluton	Grano-diorite (border)	Rhyolite dike	Granite pluton	Granite pluton	Granite pluton
Location	Fig. 3A	Fig. 3A	Fig. 3A	Fig. 3A	Fig. 3A	Fig. 3A	Fig. 3A	Fig. 3A	Fig. 3A	Fig. 3A	Fig. 3A	Fig. 3A	Fig. 3A	Fig. 3A	Fig. 3A	Fig. 3A	Fig. 3A
(Wt %)																	
SiO_2	56.29	55.91	53.73	54.78	56.74	54.84	54.81	55.15	56.81	58.85	60.85	65.12	63.62	74.03	74.60	73.78	73.49
Al_2O_3	18.17	17.52	18.60	18.51	17.93	18.38	18.30	17.53	17.24	17.40	16.74	15.17	16.07	13.85	14.25	14.54	14.95
TiO_2	0.79	0.87	0.83	0.70	0.75	0.85	0.86	0.98	0.73	0.71	0.59	0.58	0.61	0.19	0.19	0.23	0.26
Fe_2O_3	7.70	7.36	9.04	8.53	7.78	8.16	8.27	8.15	7.28	6.94	4.90	5.02	5.16	0.58	0.42	1.31	0.75
MnO	0.15	0.09	0.12	0.08	0.13	0.15	0.16	0.13	0.12	0.10	0.05	0.05	0.05	0.02	0.02	0.03	0.02
CaO	7.03	6.12	7.26	7.14	6.48	7.62	7.27	7.49	7.09	6.17	4.88	4.04	4.64	1.85	0.57	1.36	2.22
MgO	2.80	3.08	3.05	2.97	2.69	2.98	3.01	4.16	3.77	2.86	1.87	1.88	2.06	0.19	0.10	0.40	0.14
K_2O	1.31	1.89	1.10	1.46	1.33	1.17	1.22	1.11	1.78	1.93	2.43	3.60	3.14	0.14	2.35	3.39	3.11
Na_2O	3.61	3.85	3.79	3.44	3.48	3.87	3.85	3.18	3.29	3.69	3.36	3.29	3.46	7.30	6.32	4.91	5.00
P_2O_5	0.23	0.20	0.28	0.32	0.25	0.26	0.25	0.21	0.24	0.22	0.17	0.14	0.18	0.04	0.04	0.05	0.06
LOI	0.85	1.91	1.16	1.20	1.10	0.82	0.98	1.20	1.00	0.90	3.60	0.70	0.70	1.80	1.00	1.65	2.30
Total	98.93	98.79	98.96	99.13	98.66	99.09	98.98	99.29	99.35	99.77	99.44	99.59	99.69	99.99	99.86	100.00	99.99
(Ppm)																	
Ba	313	394	256	399	377	263	268	307	412	405.2	551.00	656.50	562.00	24.20	773.10	797.40	665.00
Ce	37	45	39	29.6	40	34	40	34.5	39.9	45.8	34.40	76.00	52.50	22.40	49.90	38.65	51.20
Nb	6	6	5	4.1	4.4	5	5	5.3	4.7	6.2	5.10	9.90	8.10	14.20	14.60	11.75	12.50
Ni	3	9	3	1.5	1.8	3	3	28	24	2.5	2.00	3.90	4.90	1.30	0.30	n.a.	n.a.
Rb	47	69	38	60.2	45.5	34	44	61	57.8	62.8	63.70	111.60	111.80	4.20	52.90	123.99	87.60
Sc	14	12	16	11	11	16	16	23	15	11	7.00	10.00	10.00	1.00	1.00	2.00	2.00
Sr	603	601	601	662.7	613.6	643	607	538	621.7	555.8	526.70	417.20	477.50	115.40	150.10	197.34	166.10
Th	4	6	<3	5.1	4.2	3	3	4.1	6	5.7	7.00	16.80	13.50	9.60	13.00	10.75	11.30
U	0.9	<3	0.6	1.2	0.9	0.6	0.8	1.7	1.1	1	1.90	2.20	2.60	2.70	3.60	1.74	2.20
V	116	120	126	121	126	125	117	209	142	102	75.00	76.00	81.00	8.00	7.00	8.00	13.00
Y	21	18	21	20.5	20.3	20	20	25.3	21.1	21.6	18.00	29.30	23.50	11.00	18.00	11.10	12.30
Zr	137	147	124	172.4	130.5	117	127	139.9	147.6	156.7	130.80	227.00	217.00	109.60	137.60	113.93	116.30
Cs	1.8	n.a.	1.5	1.1	1.3	1.3	1.9	1.9	2	4.3	1.20	1.50	1.90	0.50	0.70	n.a.	n.a.
Hf	3.6	n.a.	2.8	5.4	3.9	3.3	3.5	4.1	3.9	4.8	3.80	7.10	6.60	3.40	4.30	3.46	3.00
Ta	0.3	n.a.	0.2	0.3	0.4	0.2	0.2	0.4	0.4	0.5	0.50	1.00	0.70	1.30	1.60	1.40	1.50
La	18.8	17	16	13.1	17.9	15.3	17.3	14.7	18.7	19.1	15.30	33.50	23.40	10.50	19.40	20.80	28.20
Ce	41.4	45	36.9	29.6	40	34.1	39.4	34.5	39.9	45.8	34.40	76.00	52.50	22.40	49.90	38.65	51.20
Pr	5.18	n.a.	4.6	3.98	5.25	4.31	5.01	4.47	4.99	5.58	4.36	8.61	6.14	2.48	5.63	4.20	5.80
Nd	21	<22	21.5	18.9	23.1	18.1	22.2	19.3	22	24.8	18.90	32.10	24.70	8.60	18.80	11.75	17.60
Sm	4.3	n.a.	4.3	3.8	4.5	4	4.2	4.5	4.6	5	3.60	6.10	4.90	1.70	3.40	2.15	3.00
Eu	1.27	n.a.	1.45	1.32	1.18	1.23	1.25	1.26	1.13	1.23	1.13	1.08	1.05	0.22	0.69	0.60	0.60
Gd	3.09	n.a.	3.41	4.02	4.51	3.26	3.29	4.98	3.88	4.18	3.90	5.58	4.54	1.41	2.64	1.84	2.50
Tb	0.66	n.a.	0.72	0.55	0.54	0.61	0.64	0.72	0.6	0.68	0.52	0.89	0.74	0.25	0.48	0.30	0.30
Dy	3.57	n.a.	3.99	3.28	3.18	3.41	3.46	4.18	3.56	3.9	2.91	5.42	4.06	1.59	2.67	1.75	1.90
Ho	0.63	n.a.	0.79	0.66	0.63	0.63	0.79	0.8	0.68	0.8	0.57	1.06	0.84	0.33	0.60	0.35	0.40
Er	2	n.a.	1.99	2.2	1.92	1.76	1.76	2.62	2.22	2.05	1.94	2.98	2.22	0.99	1.63	1.20	1.20
Tm	0.37	n.a.	0.32	0.29	0.24	0.28	0.28	0.33	0.27	0.31	0.25	0.46	0.38	0.21	0.28	0.20	0.20
Yb	1.95	n.a.	2.13	1.94	1.82	1.62	1.81	2.23	2	2.05	1.69	2.81	2.14	1.24	1.85	1.35	1.30
Lu	0.32	n.a.	0.31	0.33	0.32	0.26	0.27	0.35	0.27	0.36	0.27	0.48	0.38	0.25	0.35	0.2	0.2

n.a. = not analyzed

plutons of southwest Mendoza that are associated with iron skarns and to intrusive rocks associated with iron skarns worldwide (cf. Meinert, 1995). They are intermediate to silicic in composition (Table 1), metaluminous, I-type (Chapell and White, 1992) (Fig. 4A, B), and subalkaline with calc-alkaline affinity (Fig. 4A, C). In SiO_2 versus total alkalis and SiO_2 versus MgO diagrams (Fig. 4A, D), the diorite samples plot in the less differentiated field, with low SiO_2 and high MgO, similar to primitive plutons associated with iron and gold skarns (Meinert, 1995). In both diagrams the granite samples that lack mafic minerals plot in the opposite side of the diorite samples (Fig. 4A, D).

The N-MORB normalized trace element patterns (Pearce, 1996) of all the Vegas Peladas igneous rocks show a negative Nb anomaly relative to Th and Ce and negative Ti anomaly relative to Zr and Y, with Zr and Y values close to 1 (Fig. 5A). These patterns are all characteristic of calc-alkaline magmas derived from a subarc mantle source, with scarce or no garnet in the source. The REE patterns of the diorite and granodiorite plutons are similar to those of the igneous rocks associated with Fe and Au skarns, whereas the granite has a pattern more similar to plutons associated with Zn skarns (Fig. 5A, B). Like other plutons associated with iron skarns of southwest Mendoza, the concentrations of trace elements and REE in the Vegas Peladas igneous rocks are similar to the Planchón-Peteroa (35°30′S) and Nevados del Chillán (36°30′S) Quaternary volcanic groups (Quaternary Volcanic Arc of the Transitional southern volcanic zone, TSVZ, 34°30′-37°S), which were emplaced in a relatively thin continental crust (~35–50 km: Davidson et al., 1988; Hildreth and Moorbath, 1988; Tormey et al., 1991; Franchini et al., 2003; Pons et al., 2007). The preliminary $^{87}Sr/^{86}Sr$ ratio of 0.704351 ± 0.000044 (Pons, 2007) is consistent with a mantle source for these rocks with little to no crustal contamination (cf. Hildreth and Moorbath, 1988).

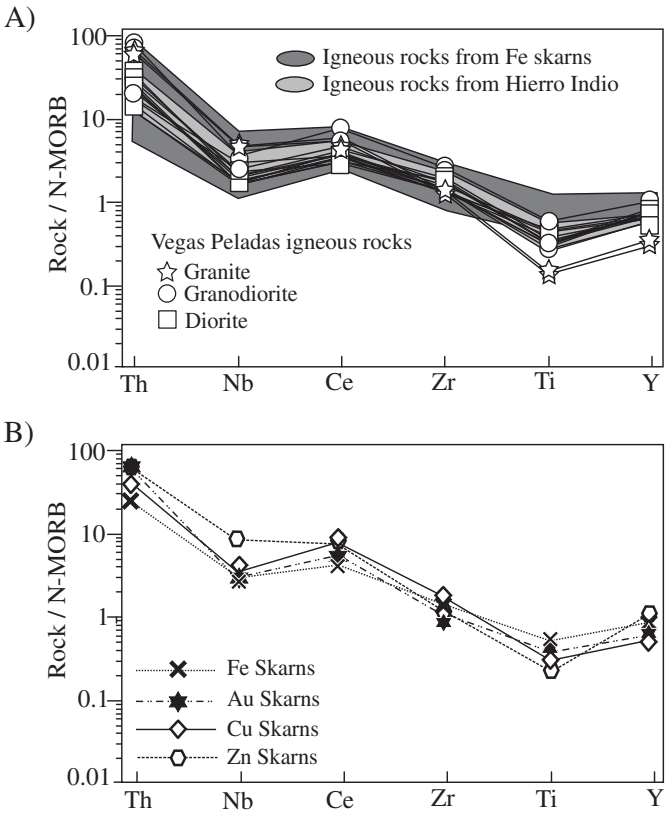

FIG. 5. A. Trace element abundance normalized to N-MORB (Pearce, 1996) for the Vegas Peladas igneous rocks; for comparison, the field of igneous rocks from Fe skarns worldwide and the Hierro Indio Fe skarn. B. The average trace element contents of igneous rocks from Fe, Au, Cu, Zn worldwide skarns (data from Meinert 1995).

Samples and Analytical Methods

This study is based on 400 samples collected from mapped outcrops. Samples were analyzed by transmitted and reflected light petrography and X-ray diffraction (Rigaku-DII-Max) at the Centro de Investigaciones de Minerales Arcillosos of the Universidad Nacional del Comahue (Neuquén, Argentina). The chemical compositions of the minerals (220 analyses) were determined by electron microprobe at the Centro de Desenvolvimento da Tecnologia Nuclear (CDTN, CNEN, Belo Horizonte, Brazil, using a Jeol-JXA- 8900 RL WD/ED microprobe), at the Servicios Científicos-Técnicos of the Universidad de Barcelona, and at the Departamento de Geología of the Universidad de Oviedo, Spain (using Cameca SX50). Microprobe analyses of igneous and alteration minerals are available in Appendices 1–7 as a digital supplement online at <http://www.geoscienceworld.org/> or, for subscribers, on the SEG website, <http://www.segweb.org>.

Microthermometric analyses of fluid inclusions (270 inclusions) in quartz, garnet, pyroxene and calcite were carried out using Linkam (–180°/+600°C) fluid inclusion cooling-heating stages at the Fluid Inclusion Laboratory of the Departamento de Geología of the Universidad Nacional del Sur, Bahía Blanca, Argentina. Homogenization temperatures higher than 550°C were measured with a Leitz Wetzlar Heating stage 1350 for melt inclusions, with Heinzinger 16-30 control system, at the Centro de Desenvolvimento da Tecnologia Nuclear, Belo Horizonte, Brazil. Synthetic standards from Bubbles Inc. were used to calibrate microthermometric analyses.

Sixteen samples of least-altered igneous rocks were analyzed for major and trace and rare earth elements by inductively coupled plasma-emission spectrometry (ICP-ES), ICP mass spectrometry (ICP-MS), and X-ray fluorescence at Alex Stewart Assayers Ltd., Ireland, at Acme Analytical Laboratories Ltd., Canada, and at the Instituto de Geociências of the Universidade de São Paulo, Brazil, respectively. Ten samples of the sedimentary rocks, hornfels and skarn were analyzed for REE concentrations at Acme Analytical Laboratories Ltd., Canada. Seven samples of the Vegas Peladas mineralized skarn were analyzed for base and precious metals by ICP-ES and for Au by fire assay (with atomic absorption finish), at Acme Analytical Laboratories, Canada.

A radiometric age for an igneous rock sample (Vegas Peladas granodiorite) was determined by $^{87}Rb/^{86}Sr$ in whole rock and in biotite at the CPGeo-Centro de Pesquisas Geocronológicas, Instituto de Instituto de Geociências of the Universidade de São Paulo, Brazil.

Selected silicates, carbonates and oxides were analyzed for $\delta^{18}O$, δD, and $\delta^{13}C$, as appropriate, at the Servicio de Isótopos Estables, Universidad de Salamanca, using two SIRA-II, gaseous source, and dual inlet mass spectrometers. Samples

were prepared by handpicking and then converted to a suitable gas in dedicated extraction lines. Oxygen from silicates was analyzed as CO_2 produced by laser fluorination, mostly following Sharp (1990), using a 25-W CO_2 laser and a dedicated extraction and purification line. Hydrogen extraction for isotopic analyses was based on the work of Godfrey (1962). Minerals were melted by induction heating and the water released was reduced to H_2 gas over hot depleted U. Carbonates were analyzed as CO_2 produced by acid reaction using 103 percent H_3PO_4 (McCrea, 1950). Isotopic results are reported in the familiar δ notation relative to SMOW (Standard Mean Ocean Water) for oxygen and hydrogen and PDB (Pee Dee Belemnite) for carbon. Repeated analyses of international and internal reference materials gave average reproducibilities better than ±0.02 per mil $\delta^{13}C$ and ±0.12 per mil $\delta^{18}O$ for C and O in carbonates, ±0.2 per mil for O by laser fluorination, and ±1 for D/H.

Alteration and Mineralization

On the northeast side of Las Minas Hill, several zones with hydrothermal alteration and Fe mineralization crop out discontinuously for 3 km parallel to Vegas Peladas Creek (Fig. 3B). The field relationships between the sedimentary and the igneous rocks and the alteration and Fe mineralization reveal the following zonation: (1) hornfels and Fe skarns associated with the diorite pluton, (2) hornfels and skarn with incipient Fe mineralization associated with the granite pluton and related rhyolite dikes and sills, (3) hydrothermal alteration in the margin of the granodiorite pluton and associated dikes, and (4) hydrothermal alteration with disseminated Fe mineralization restricted to the later andesite dikes. The most important is the skarn related to the diorite pluton. The distribution of alteration and mineralization is shown in Figure 3B.

Fe skarn associated with the diorite pluton

There are six main outcrops of iron mineralization associated with diorite (numbered from 1 to 6; Fig. 3B). They consist of bands and lenses concordant with the exoskarns that replace the calcareous facies of the Jurassic sedimentary rocks (Calabozo Formation). Other smaller iron bodies are hosted in the exoskarn that replaces the less reactive sedimentary rocks (Puchenque Formation) and in the altered igneous rock. The banded bodies are localized in the exoskarn next to the contact with the diorite pluton (<30 m wide). The most important is the no. 1 body in Figure 3B. Based on old mining activity it is 30-m long × 5-m thick and comprises epidote + quartz exoskarn accompanying massive magnetite (Arrospide, 1972; Pons, 2007). At present, it is partially covered by debris. The rest of the iron outcrops (no. 2–6) are smaller, between 2 and 6 m^2. The diorite pluton is cut by veins, veinlets, and stockwork, with iron mineralization next to the contact with the sedimentary rocks and the granodiorite pluton (Fig. 3B). Outcrop no. 7 is a mineralized breccia located in a shear zone next to the contact with the granite pluton (Fig. 3B). Historical Fe production was small and total resources are visually estimated at less than 10 Mt.

This iron skarn is characterized by the following elements: (1) a ubiquitous metamorphic halo of banded hornfels after sedimentary rocks around the diorite stock, (2) alteration of the diorite pluton and dike margins (endoskarn) with variable morphologies, and (3) zoned exoskarn with prograde and retrograde paragenesis (in space and time), concordant mantle, veins, and lenses of iron mineralization. The contacts between the igneous and sedimentary rocks, bedding planes, and joints all served as channel ways for hydrothermal fluid flow.

Alteration in the diorite: The margin of the diorite pluton contains ~10 vol percent alteration minerals (Figs. 6–8). The primary mafic minerals are replaced by actinolite ± chlorite ± calcite ± magnetite ± titanite and the magmatic magnetite is rimmed by titanite. The plagioclase has patches of orthoclase ($Or_{87–93}$; sample 2696, Table 2) ± epidote ± calcite. Pyrite occurs as fine-grained disseminations (1 vol %). In contact with the sedimentary rocks, the diorite is replaced by a massive, 0.5- to 2-m-thick, grayish white alteration of orthoclase + quartz (Figs. 6, 7). Superimposed on these earlier minerals are patches of quartz ± epidote ± actinolite ± pyrite (Figs. 6, 7). Another less common texture consists of calcareous xenoliths in the diorite replaced by a core of red-brown garnet with grayish white orthoclase + quartz halos partially replaced by epidote ± chlorite. Dikes and sills that emanate from the diorite pluton have thin, light green epidote + calcite ± alkali feldspar selvages (Fig. 8). An igneous anastomosing breccia (>15 cm thick) occurs at the contact between the thickest (>3 m thick) sills and dikes and the less reactive sedimentary rocks. This breccia contains angular fragments of hornfels of variable size and a leached igneous matrix with alkali feldspar-rich alteration (Fig. 8). In the diorite margin there are numerous veins, joints, and miarolitic cavities filled or coated by amphibole ± quartz ± magnetite ± epidote ± alkali feldspar (Fig. 6). The veins are zoned from a quartz ± magnetite center, an amphibole ± epidote border and an envelope of white alkali feldspar in the igneous wall rocks. Close to the granodiorite, the diorite hosts numerous veins and pockets of massive magnetite that locally develops stockwork.

Alteration in the sedimentary rocks: At the contact with the diorite pluton, the Puchenque and Calabozo Formations have been transformed to hornfels (quartz-feldspar, clinopyroxene, biotite, and sericite) and marble, respectively, forming a metamorphic halo 800 m wide (Figs. 3B, 6–8).

The exoskarn crops out on the southwest side of the creek, with a maximum thickness of 60 m. It replaces marble and hornfels as concordant bands and discordant veins with the following zones: (1) an inner zone of clinopyroxene + magnetite + quartz or brown garnet ± quartz, (2) an intermediate zone of massive garnet ± clinopyroxene, (3) external veins with a similar assemblage, (4) retrograde assemblages with epidote + magnetite and epidote + hematite (or magnetite) superimposed on the inner and intermediate zone, respectively, (5) external, retrograde amphibole-rich zones with hematite (or magnetite) replacing the prograde veins and cutting the hornfels, and (6) ubiquitous, late albite($Ab_{96–98}$) ± epidote ± quartz ± calcite ± chlorite ± pyrite ± titanite (Figs. 3B, 6–8) affecting all earlier alteration assemblages.

The prograde zones are exposed as parallel bands, 1.5 km long and ~50 m thick, adjacent to the diorite pluton and its dikes (Figs. 3B, 6–8). The inner clinopyroxene-rich zone (Fig. 7) along with massive magnetite as bands, lenses, and veins replaces siliciclastic rocks close to the diorite contact. The inner garnet-rich zone is at least 450 m long but based on

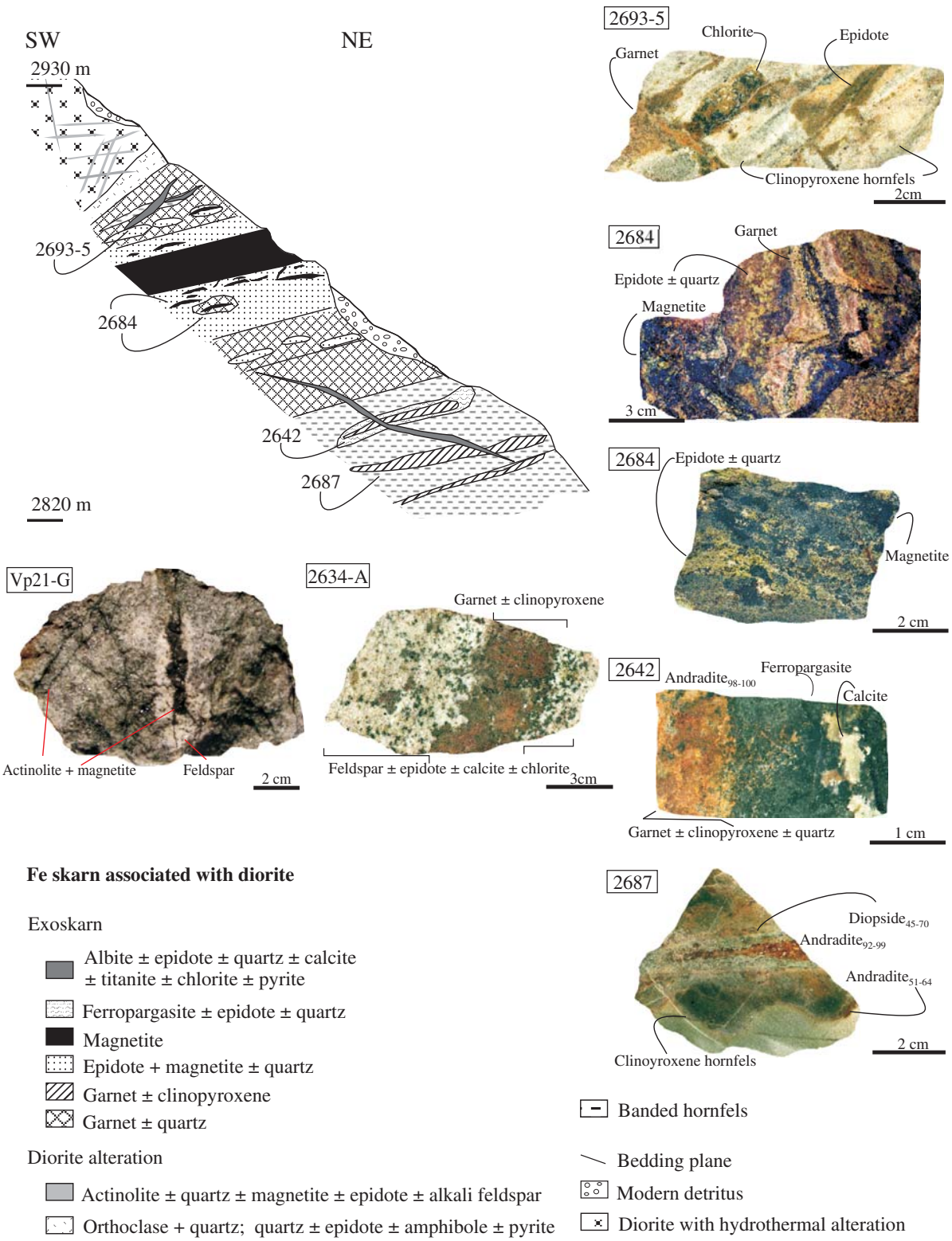

FIG. 6. Schematic southwest-northeast profile of the Fe skarn associated with the diorite shown in Fig. 3B, including photographs of the main alteration and mineralization styles in the profile. Sample 2693-5: garnet exoskarn and its late retrograde alteration to epidote ± chlorite controlled by joints in the pyroxene hornfels. Sample 2684: retrograde magnetite ± epidote ± quartz alteration of the proximal garnet exoskarn zone. Sample 2642: intermediate garnet ± clinopyroxene exoskarn replaced by ferropargasite and late calcite. Sample 2687: intermediate garnet ± clinopyroxene exoskarn cutting pyroxene hornfels. The location of the samples Vp 21-G: actinolite ± quartz ± magnetite ± epidote ± alkali-feldspar replacing diorite and 2634-A: intermediate garnet ± clinopyroxene exoskarn partially altered to alkali-feldspar ± epidote ± calcite ± chlorite are shown in Figure 3B.

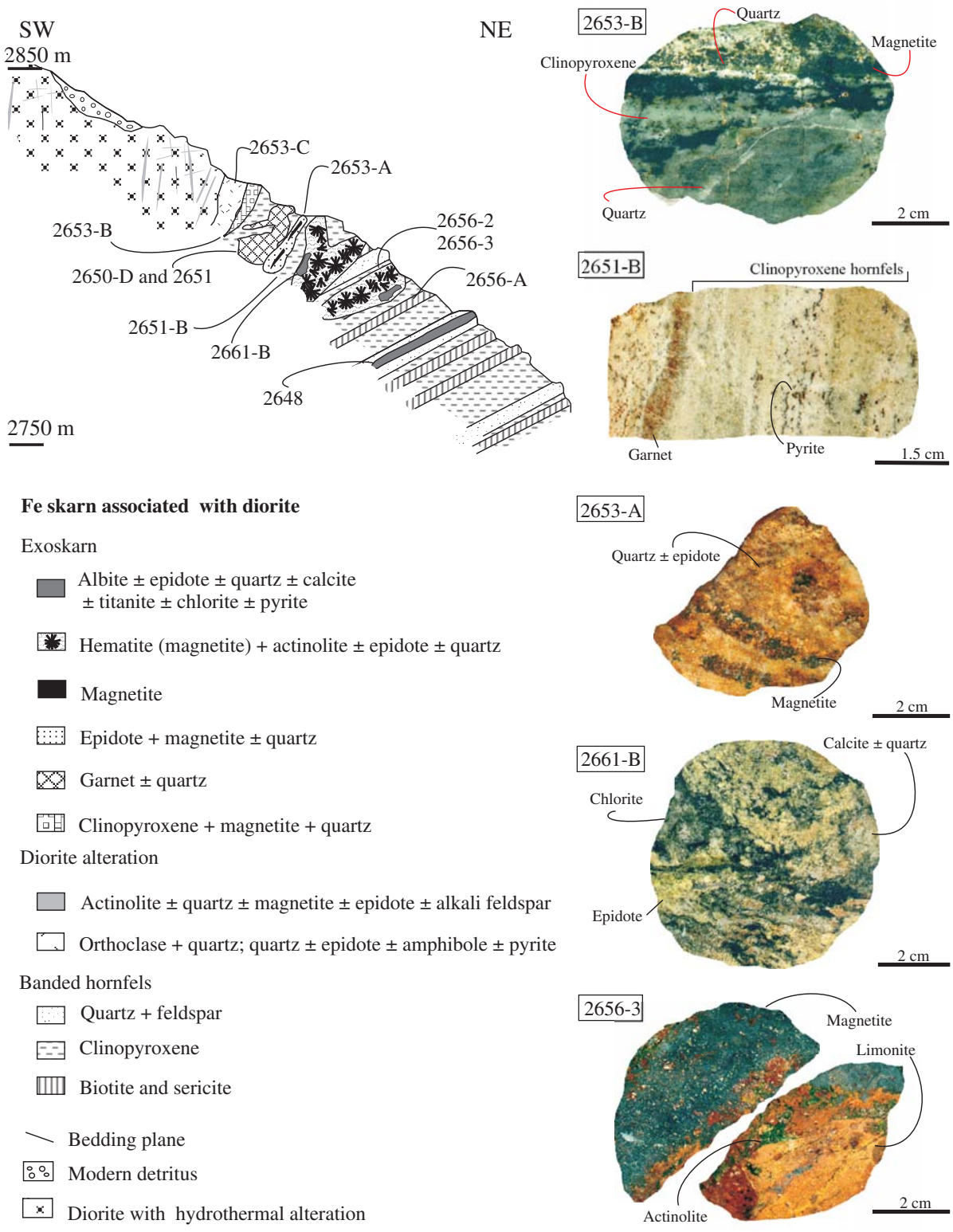

FIG. 7. Schematic southwest-northeast profile of the Fe skarn associated with the diorite shown in Figure 3B, including photographs of the main alteration and mineralization styles in the profile. Sample 2653-B: inner clinopyroxene + magnetite + quartz exoskarn. Sample 2651-B: garnet exoskarn vein cutting pyroxene hornfels. Sample 2653-A: epidote + magnetite ± quartz overprinting the inner exoskarn. Sample 2661-B: epidote ± quartz ± calcite ± chlorite replaces the amphibole-rich alteration. Sample 2656-3: distal, partially oxidized magnetite (after hematite) veins with actinolite envelopes.

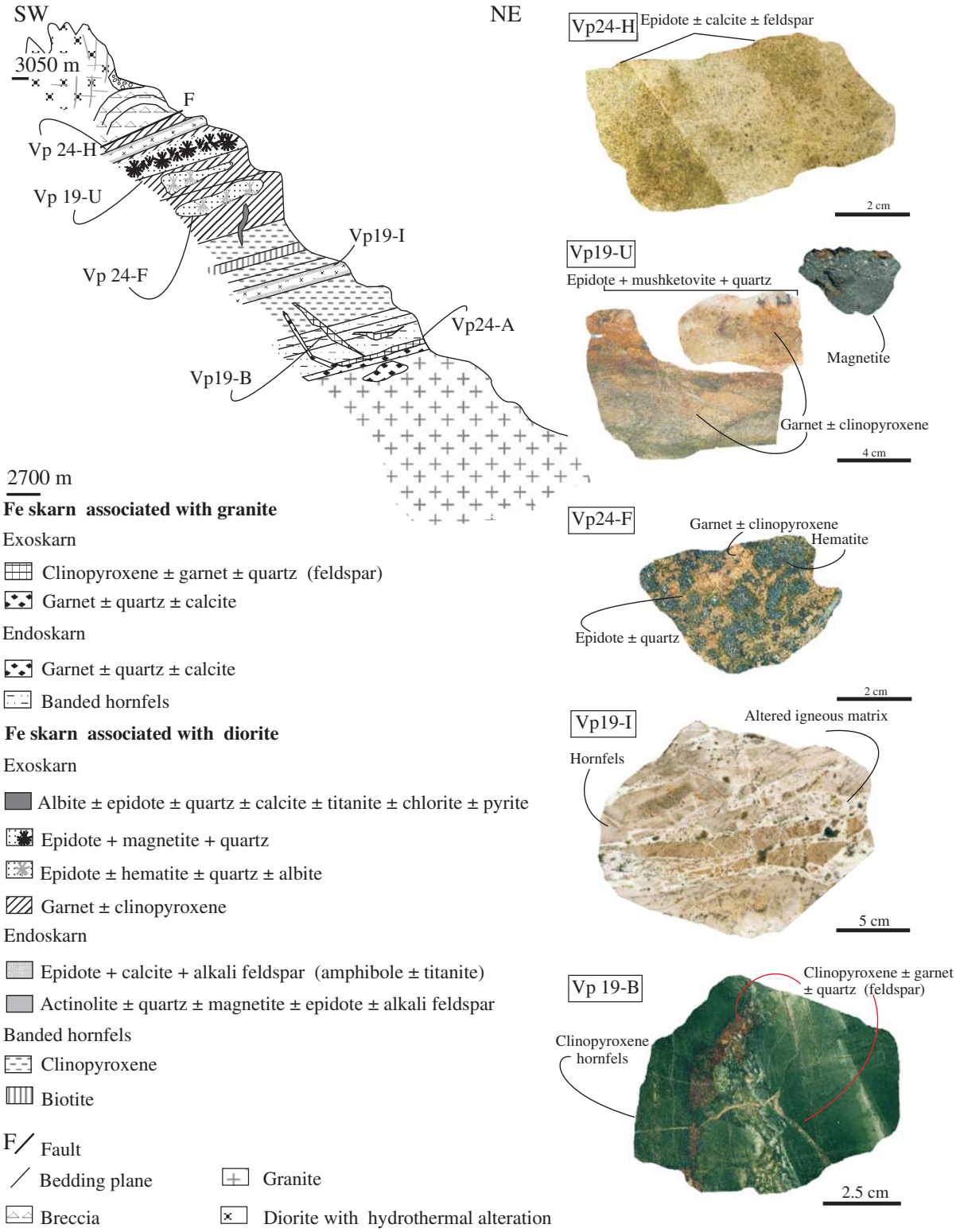

FIG. 8. Schematic southwest-northeast profile of the Fe skarn associated with the diorite and the skarn associated with granite shown in Fig. 3B, including photographs of the main alteration and mineralization styles in the profile. Sample VP24-H: epidote ± calcite ± alkali feldspar endoskarn envelope replacing a diorite dike. Sample VP19-U: intermediate garnet ± pyroxene exoskarn partially altered to epidote ± quartz and distal magnetite. Sample VP24-F: intermediate garnet ± pyroxene exoskarn partially replaced by specular hematite clots rimmed by epidote ± quartz and late calcite ± chlorite. Sample VP19-I: breccia with angular fragments of hornfels of variable size in an alterated and leached igneous matrix. Sample VP19-B: veins of clinopyroxene ± garnet ± quartz (feldspar) cutting clinopyroxene hornfels from the exoskarn associated with the granite.

TABLE 2. Representative Electron Microprobe Analyses of Alkalic Feldpars from the Skarn Associated with Diorite and from the Endoskarn Associated with Granite

Alteration	Hydrothermal alteration		Exoskarn			Exoskarn							Endoskarn			
Sample no.	2696-1	2696-2	2648-6		2648-4	2701F-1			2701F-2-1				2629-B-2			
Location	Fig. 3A		Fig. 7			Fig. 3B							Fig. 3A			
(Wt %)																
SiO_2	64.21	63.25	69.34	61.29	57.93	72.53	66.47	66.31	67.73	68.73	68.39	68.23	66.54	63.89	63.53	61.34
TiO_2	0.01	0.07	0.027	0.003	0.010	0.001	n.d.	0.025	n.d.	n.d.	n.d.	n.d.	0.02	n.d.	n.d.	n.d.
Al_2O_3	17.72	17.41	20.90	19.45	15.80	17.10	19.95	20.99	20.12	19.70	19.94	20.50	20.63	22.14	22.48	21.06
MnO	0.04	0.05	0.09	0.00	0.00	0.00	0.00	0.00	0.03	0.02	0.00	0.00	0.00	0.01	0.01	0.00
MgO	0.02	1.71	0.02	0.00	0.00	0.02	0.40	0.00	0.00	0.01	0.01	0.00	0.08	0.00	0.00	0.02
FeO	0.35	0.99	0.07	0.01	0.03	0.06	0.89	0.08	0.03	0.06	0.03	0.08	0.11	0.03	0.17	0.25
CaO	0.07	1.36	0.42	0.53	0.22	1.03	1.21	1.92	1.40	0.49	0.96	0.94	1.96	3.82	4.03	3.62
Na_2O	0.73	0.63	6.20	10.30	6.05	9.06	10.73	10.78	10.83	11.67	11.15	11.33	10.75	9.96	9.37	10.27
K_2O	15.22	13.57	0.03	0.05	0.01	0.11	0.18	0.16	0.10	0.05	0.13	0.08	0.18	0.10	0.19	0.09
Total	98.40	99.12	97.1	91.6	80.1	99.9	99.8	100.3	100.2	100.7	100.6	101.2	100.31	99.95	99.80	96.66
Cations based on 32 oxygens																
Si	12.05	11.81	12.17	11.71	12.36	12.52	11.73	11.63	11.83	11.94	11.89	11.81	11.67	11.31	11.26	11.28
Ti	0.00	0.01	0.00	0.00	0.00	0.00	0.00	0.01	0.00	0.00	0.00	0.00	0.00	0.00	0.00	0.00
Al	3.92	3.83	4.32	4.38	3.98	3.48	4.15	4.34	4.15	4.03	4.09	4.18	4.27	4.62	4.70	4.57
Mn	0.01	0.01	0.01	0.00	0.00	0.00	0.00	0.00	0.00	0.00	0.00	0.00	0.00	0.00	0.00	0.00
Mg	0.00	0.48	0.01	0.00	0.00	0.01	0.10	0.00	0.00	0.00	0.00	0.00	0.02	0.00	0.00	0.01
Fe^{+2}	0.05	0.15	0.01	0.00	0.01	0.01	0.13	0.01	0.00	0.01	0.00	0.01	0.02	0.01	0.03	0.04
Ca	0.01	0.27	0.08	0.11	0.05	0.19	0.23	0.36	0.26	0.09	0.18	0.18	0.37	0.72	0.77	0.71
Na	0.27	0.23	2.09	3.79	2.49	3.03	3.67	3.67	3.67	3.93	3.76	3.80	3.66	3.42	3.22	3.66
K	3.64	3.23	0.01	0.01	0.00	0.02	0.04	0.03	0.02	0.01	0.03	0.02	0.04	0.02	0.04	0.02
Orthoclase	92.89	86.58	0.29	0.32	0.15	0.77	1.03	0.86	0.57	0.27	0.72	0.42	1.00	0.52	1.09	0.46
Albite	6.77	6.13	96.07	96.92	97.87	93.36	93.19	90.26	92.81	97.45	94.75	95.20	89.94	82.08	79.91	83.30
Anortite	0.34	7.29	3.64	2.76	1.98	5.87	5.78	8.88	6.62	2.28	4.53	4.39	9.06	17.40	19.00	16.24

n.d. = not detected

skarn fragments in surface float, may be more extensive. In outcrop, it is massive and brown red (Fig. 6). In thin section, garnet crystals have numerous clinopyroxene and quartz inclusions from the hornfels, complex twins, and optical zonation; the cores are isotropic and greenish brown, and the intermediate and external bands are yellowish brown and anisotropic. Microprobe analyses of garnet crystals show a wide compositional range ($Ad_{31–89}$ $Py_{0.3–2}$; Fig. 9A) as well as zonation of individual crystals from cores of intermediate composition (~Ad_{45}) to more andraditic rims (~Ad_{100}).

The intermediate and outer zones crop out at 15 and 60 m from the diorite pluton, respectively, and are best developed where this alteration replaces marble (Calabozo Formation) as massive bands up to 10 m thick (Fig. 8). The outer zone consists of garnet ± clinopyroxene bands, veins, and veinlets that replace and cut the less reactive banded hornfels (Puchenque Formation) (Fig. 6). The intermediate and outer zones contain three types of garnet: (1) massive bands of light-brown garnet with garnet crystals that are poikilitic (with clinopyroxene hornfels minerals), anisotropic, with concentric zoning and complex twins ($Ad_{38–51}$ $Py_{1–2}$; is similar to that of the inner zone; Fig. 9A); (2) thin bands and veins of isotropic, brown garnet of andradite composition ($Ad_{92–100}$ $Py_{0–0.1}$; Fig. 9A) that cut the previous garnet; (3) a green to colorless, anisotropic garnet that forms concentric halos around the isotropic garnet. The clinopyroxene ($Di_{24–70}$ $Jo_{1–4}$; Fig. 9B) occurs as euhedral to subhedral and colorless crystals that fill interstices between the garnet in the intermediate zone or as discontinuous selvages around isotropic garnet veins in the external zone (Fig. 6).

The epidote + magnetite ± quartz assemblage replaces the inner garnet-rich zone (Fig. 6), and the epidote ± hematite (or mushketovite = magnetite after specular hematite) ± quartz ± albite ($Ab_{90–98}$; sample 2701-F, Table 2; Fig. 8) assemblage replaces the intermediate zone. In thin section, epidote is pseudomorphous after garnet; it fills interstices and veins along with quartz, albite and hematite or magnetite (after hematite). Albite with specular hematite forms selvages on the garnet ± clinopyroxene bands. This alteration becomes pervasive adjacent to the massive magnetite or hematite bands (Figs. 6, 8).

The amphibole- rich assemblages consist of ferropargasite (Fig. 10) ± epidote ± quartz and hematite (partly replaced by magnetite) + actinolite (Fig. 10) ± epidote ± quartz. They replace exoskarn veins in hornfels and extend outward into the hornfels along joints and bedding planes (Figs. 6, 7). In both assemblages, epidote and granular quartz replace garnet as veins and patches. Ferropargasite crystals replace early clinopyroxene, which locally is preserved in the amphibole core. Actinolite forms the selvages of the specular hematite (partly replaced by magnetite) veins (Fig. 7) and contains microinclusions of iron oxides and quartz.

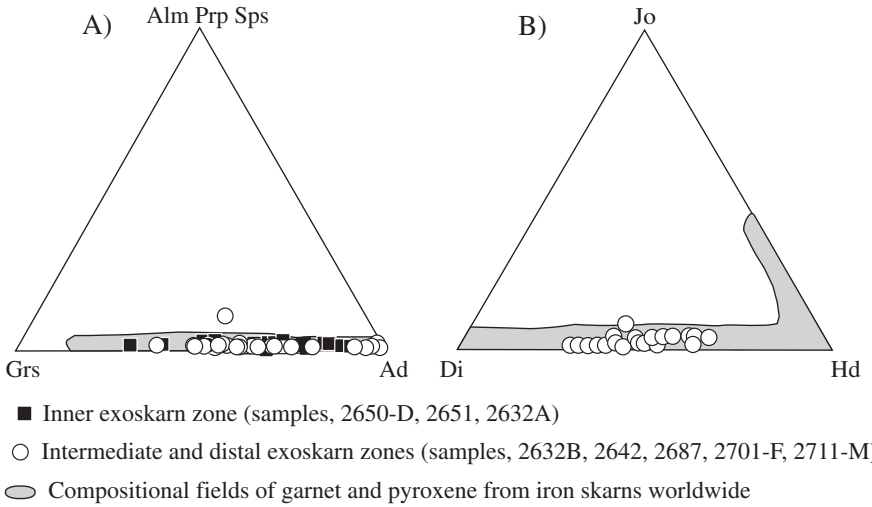

FIG. 9. A. Composition of garnet (samples 2650-D, 2651, 2687, 2632-A, 2632-B, 2711-M and 2701-F; Figs. 3B, 6, 7) and B- of clinopyroxene (samples 2642 and 2687; Fig. 6) from the Vegas Peladas exoskarn associated with diorite. The compositional fields for clinopyroxene and garnet in Fe skarn deposits worldwide (Meinert et al., 2005) are shown in both diagrams for comparison. Ad = andradite, Alm = almandine, Di = diopside, Grs = grossularite, Hd = hedenbergite, Jo = johannsenite, Prp = pyrope, Sps = spessartine.

The latest albite-rich (Ab_{96-98}; sample 2648, Table 2) alteration fills open spaces and veins and forms patches that replace and cut previous alteration assemblages (Figs. 6, 7). This alteration has a strong structural control along joints and extends beyond skarn alteration into fresh host rocks (Fig. 6).

Mineralization: The main iron ores in Vegas Peladas skarns consist of magnetite and hematite. Magnetite is closely associated and in textural equilibrium with quartz, epidote, and amphibole in endoskarn and with clinopyroxene in the exoskarn (Figs. 6, 7). However, the largest massive magnetite orebodies (30 m long × 5 m thick) occur with epidote and quartz replacing the prograde inner garnet-rich exoskarn zone (Fig. 6). This massive magnetite contains between 89 and 92 wt percent Fe_2O_3 + FeO, with minor SiO_2, MgO, CaO, Na_2O, and K_2O due to calc-silicate mineral inclusions (Table 3). MnO concentration in magnetite increases from core (below detection) to rim (0.22 wt %: Table 3). Most hematite occurs with epidote ± quartz ± albite (90–98) filling

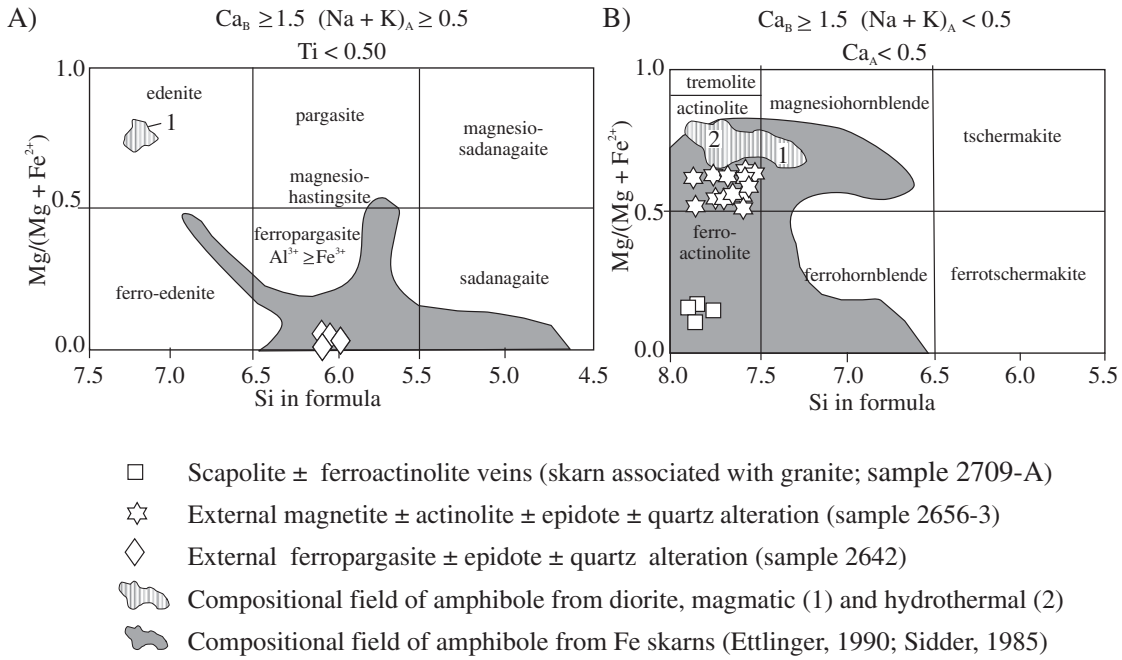

FIG. 10. Composition of amphibole from the Vegas Peladas retrograde alteration stages associated with diorite (sample 2642, Fig. 6; sample 2656-3, Fig. 7) and granite (sample 2709-A, Fig. 12). Amphibole with A) $(Na + K)_A \geq 0.5$ and Ti < 0.50 and B) with $(Na + K)_A < 0.5$ and $Ca_A < 0.5$.

TABLE 3. Representative Electron Microprobe Analyses of Magnetite and Mushketovite from the Exoskarn Associated with Diorite in the Vegas Peladas District

Sample no.	2711M					2656-3											
Location	Fig. 3B					Fig. 7											
Mineral	Magnetite					Magnetite (after hematite)											
Crystal	1-core	1-rim	2-core	2-rim	3-core	1-core	1-rim	1-rim	2-core	2-rim	2-rim	3-core	3-rim	3-rim	4-core	4-rim	4-rim
(Wt %)																	
SiO_2	2.87	0.88	0.17	0.18	2.29	n.a.	n.a.	n.a.	n.a.	n.a.	n.a.	n.a.	n.a.	n.a.	n.a.	n.a.	n.a.
TiO_2	n.d.	n.d.	n.d.	0.06	0.04	0.04	0.04	0.04	0.04	0.03	0.05	0.02	0.02	n.d.	0.01	0.01	0.04
Al_2O_3	0.17	0.08	0.02	0.04	0.09	0.15	0.12	0.17	0.40	0.24	0.21	0.33	0.28	0.45	0.19	0.12	0.25
Fe_2O_3	35.61	38.29	38.80	39.07	37.00	41.88	41.87	41.77	41.79	41.88	42.38	42.13	42.30	41.49	42.30	41.65	41.82
FeO	50.99	52.78	52.50	52.75	52.56	56.50	56.48	56.41	56.49	56.56	57.15	56.87	57.12	56.14	57.13	56.20	56.49
MnO	n.d.	0.08	n.d.	0.22	n.d.	0.14	0.15	0.06	0.10	0.12	0.12	0.05	0.03	0.06	0.05	0.08	0.09
MgO	0.15	0.01	n.d.	0.01	0.10	n.d.	0.01	n.d.	0.03	n.d.	0.02	0.01	0.03	0.01	n.d.	0.01	0.01
CaO	0.69	0.16	0.02	0.08	0.50	n.a.	n.a.	n.a.	n.a.	n.a.	n.a.	n.a.	n.a.	n.a.	n.a.	n.a.	n.a.
K_2O	0.10	0.04	0.01	0.01	0.08	n.a.	n.a.	n.a.	n.a.	n.a.	n.a.	n.a.	n.a.	n.a.	n.a.	n.a.	n.a.
Na_2O	0.16	n.d.	0.01	0.01	0.07	n.a.	n.a.	n.a.	n.a.	n.a.	n.a.	n.a.	n.a.	n.a.	n.a.	n.a.	n.a.
ZnO	n.a.	n.a.	n.a.	n.a.	n.a.	0.01	n.d.	0.09	n.d.	n.d.	0.03	0.01	n.d.	n.d.	0.01	0.02	0.02
NiO	0.01	n.d.	0.06	n.d.	n.d.	0.01	n.d.	n.d.	n.d.	n.d.	0.02	0.04	0.03	n.d.	n.d.	n.d.	0.01
CoO	n.a.	n.a.	n.a.	n.a.	n.a.	n.d.	n.d.	0.01	0.01	n.d.	0.02	0.01	n.d.	0.07	0.03	n.d.	0.01
MoO_3	n.a.	n.a.	n.a.	n.a.	n.a.	n.d.	n.d.	0.03	n.d.	n.d.	n.d.	n.d.	n.d.	0.05	n.d.	n.d.	0.03
Cr_2O_3	n.d.	n.d.	0.02	n.d.	0.05	n.a.	n.a.	n.a.	n.a.	n.a.	n.a.	n.a.	n.a.	n.a.	n.a.	n.a.	n.a.
Total	90.74	92.32	91.60	92.43	89.06	94.53	94.48	94.38	94.69	94.64	95.75	95.25	95.57	94.10	95.49	93.92	94.59
Cations based on 32 oxygens																	
Si	1.32	0.42	0.08	0.08	1.04	0.00	0.00	0.00	0.00	0.00	0.00	0.00	0.00	0.00	0.00	0.00	0.00
Ti	0.00	0.00	0.00	0.01	0.01	0.01	0.01	0.01	0.01	0.00	0.01	0.00	0.00	0.00	0.00	0.00	0.01
Al	0.09	0.05	0.01	0.02	0.05	0.08	0.06	0.09	0.21	0.13	0.11	0.17	0.15	0.24	0.10	0.07	0.13
Fe^{3+}	14.21	15.41	15.89	15.87	14.57	15.94	15.95	15.93	15.85	15.91	15.91	15.88	15.90	15.84	15.93	15.95	15.90
Fe^{2+}	28.68	30.97	31.77	31.63	29.43	31.80	31.83	31.79	31.61	31.75	31.72	31.65	31.71	31.56	31.82	31.86	31.71
Mn	0.00	0.03	0.00	0.09	0.00	0.05	0.06	0.02	0.04	0.04	0.04	0.02	0.01	0.02	0.02	0.03	0.03
Mg	0.10	0.01	0.00	0.01	0.07	0.00	0.00	0.00	0.02	0.00	0.01	0.01	0.02	0.01	0.00	0.00	0.01
Ca	0.34	0.08	0.01	0.04	0.25	0.00	0.00	0.00	0.00	0.00	0.00	0.00	0.00	0.00	0.00	0.00	0.00
Na	0.14	0.00	0.01	0.01	0.06	0.00	0.00	0.00	0.00	0.00	0.00	0.00	0.00	0.00	0.00	0.00	0.00
K	0.06	0.02	0.01	0.01	0.04	0.00	0.00	0.00	0.00	0.00	0.00	0.00	0.00	0.00	0.00	0.00	0.00
Zn	0.00	0.00	0.00	0.00	0.00	0.00	0.00	0.03	0.00	0.00	0.01	0.00	0.00	0.00	0.00	0.01	0.01

Fe^{3+}/Fe^{2+} calculated according to Droop (1987)
n.a. = not analyzed, n.d. = not detected

veins and irregular pockets that replace the prograde intermediate (garnet ± clinopyroxene) exoskarn zone (Fig. 8), and much of this hematite was later replaced by magnetite (Fig. 8). Distal, iron-rich orebodies consist of hematite (partly replaced by magnetite) with amphibole envelopes (Fig. 7). Magnetite that has replaced by hematite has higher Fe_2O_3 + FeO concentrations (between 94 and 96 wt %: Table 3) than the early magnetite and has low MnO (up to 0.15 wt %) concentrations (Table 3). The geochemistry of seven Fe ore samples from different locations includes anomalous Cu (240 ppm) and Ag (2.9 g/t) in an external amphibole vein. Pyrite concentration in the entire skarn averages 1 vol %. Supergene alteration is minor and occurs as incipient oxidation of magnetite along cleavage surfaces and fractures and also as thin veinlets of limonite and halos of iron oxides and hydroxides replacing pyrite.

REE geochemistry of skarn

The distribution of rare earth elements in the fresh and altered sedimentary rocks (hornfels and exoskarns) is shown in Figure 11. Fresh calcareous sandstone and wackestone, quartz feldspar hornfels, and pyroxene hornfels have similar REE patterns and all show negative Eu anomalies (highest in the sedimentary protolith). The garnet-rich inner exoskarn zone is enriched in the intermediate and heavy rare earth elements (e.g., Sm and Yb) compared to the sedimentary protoliths and the hornfels. In contrast, the retrograde assemblages in the exoskarn are depleted in the REE. The magnetite ± amphibole-rich assemblage has the lowest REE concentration, and all retrograde assemblages have positive Eu anomalies, which are highest in the sample with abundant magnetite and epidote.

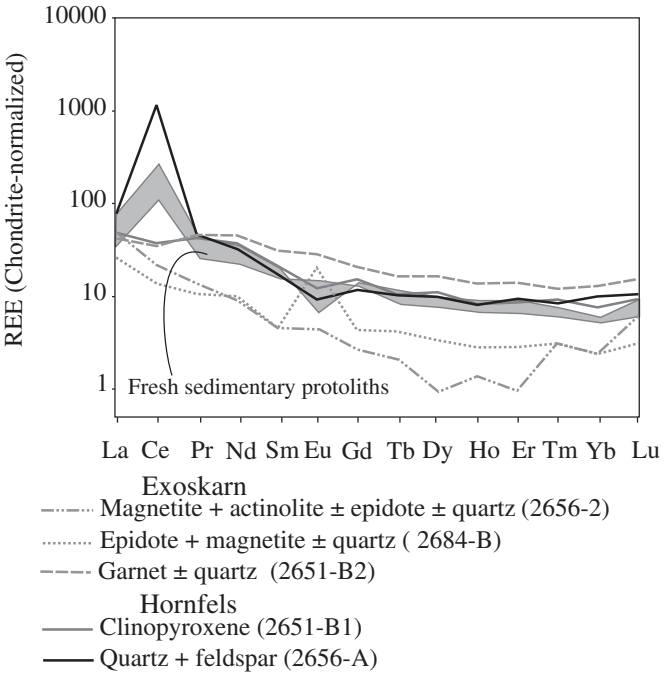

FIG. 11. Rare earth patterns (normalized to chondrite; Boynton, 1989) of the hornfels and exoskarn associated with diorite with the patterns of the fresh sedimentary rocks.

Iron skarn associated with the granite pluton

On the northeast flank of the Cerro Las Minas Hill, the granite pluton with numerous rhyolite dikes and sills intruded the marble, hornfels, and the iron skarn associated with diorite (Figs. 3B, 12). These igneous rocks formed a metamorphic aureole only a few meters wide (Figs. 3B, 8) with clinopyroxene, amphibole, and scapolite hornfels and a superposed zoned skarn with iron mineralization (Fig. 12).

Alteration of the granite and rhyolite: The margins of the granite pluton and dikes have minor hydrothermal alteration (10 vol %) including chlorite ± calcite (titanite) replacement of mafic minerals, calcite ± epidote replacement of feldspar cores, and patches and veins of albite ($Ab_{80–90}$, sample 2629-B2: Table 2) replacing feldspar. Pyrite (1 vol %) is disseminated in the altered rock. Chemical analyses of the granite and a rhyolite dike (Table 1) located near the skarn are consistent with the petrographic observations; both rocks are depleted in K_2O and enriched in Na_2O compared to least altered igneous rocks.

Near the contact with the sedimentary hosts, the granite pluton and the rhyolite dikes contain lenses and veins of garnet ± quartz ± alkali feldspar endoskarn (Fig. 12), and the rhyolite sills are replaced by scapolite ($Me_{28–36}$, sample 2709-B: Table 4) ± albite ± clinopyroxene endoskarn with envelopes of green clinopyroxene (Fig. 12).

Alteration of the sedimentary rocks: In contact with the endoskarn, the marble is replaced by a zoned exoskarn with an inner brown garnet ± clinopyroxene ± quartz zone, an outer zone of green garnet ($Ad_{30–81}$ $Py_{0–1}$, Fig. 13A) + clinopyroxene ($Di_{82–93}$ $Jo_{4–2}$, Fig. 13B) + quartz, and lenses, bands, and veins of scapolite ± clinopyroxene ($Di_{18–4}$ $Jo_{9–2}$, Fig. 13B) ± garnet that replace the banded hornfels (Fig. 12). Numerous scapolite ($Me_{25–36}$, sample 2709-A: Table 4) ± ferroactinolite (Fig. 10) ± pyrite veins cut the exoskarn and marble (Fig. 12). Veins and veinlets of chlorite ± calcite ± quartz ± hematite (partly replaced by magnetite) ± epidote (pyrite) cut earlier alteration and extend outward into the fresh sedimentary rocks (Fig. 12). The mineralized bodies associated with rhyolite dikes that intrude marble are small in size (1.5 × 6 m) and consist of lenses and veins of hematite (partly replaced by magnetite) (Fig. 12). At the contact with the granite and the early iron skarn, there is a breccia (Fig. 12) consisting of fragments of brown garnet ± pyroxene exoskarn cemented by magnetite ± quartz ± epidote.

In the middle of the Vegas Peladas Valley, in the southwest margin of the creek, the granite cupola crops out in contact with a barren and zoned skarn (endoskarn + exoskarn) a few meters wide (Fig. 8). The endoskarn consists of veins of light brown garnet ± quartz ± calcite. In the contact with the endoskarn, the sedimentary protolith is replaced by an inner zone of massive brown garnet ± quartz ± calcite that grades to an intermediate zone of clinopyroxene ± garnet ± quartz (feldspar) and extends outward as veins cutting pyroxene hornfels (Fig. 8). On the northeast margin of the creek, in the contact with granite dikes and sills, there is an exoskarn with scapolite + $Ad_{10–83}$ $Py_{1–1}$ ± $Di_{43–96}$ $Jo_{3–1}$ (Fig. 13A, B).

Fluid Inclusions

Secondary fluid inclusions are abundant in igneous quartz in diorite, granodiorite, and granite, and also in quartz of the

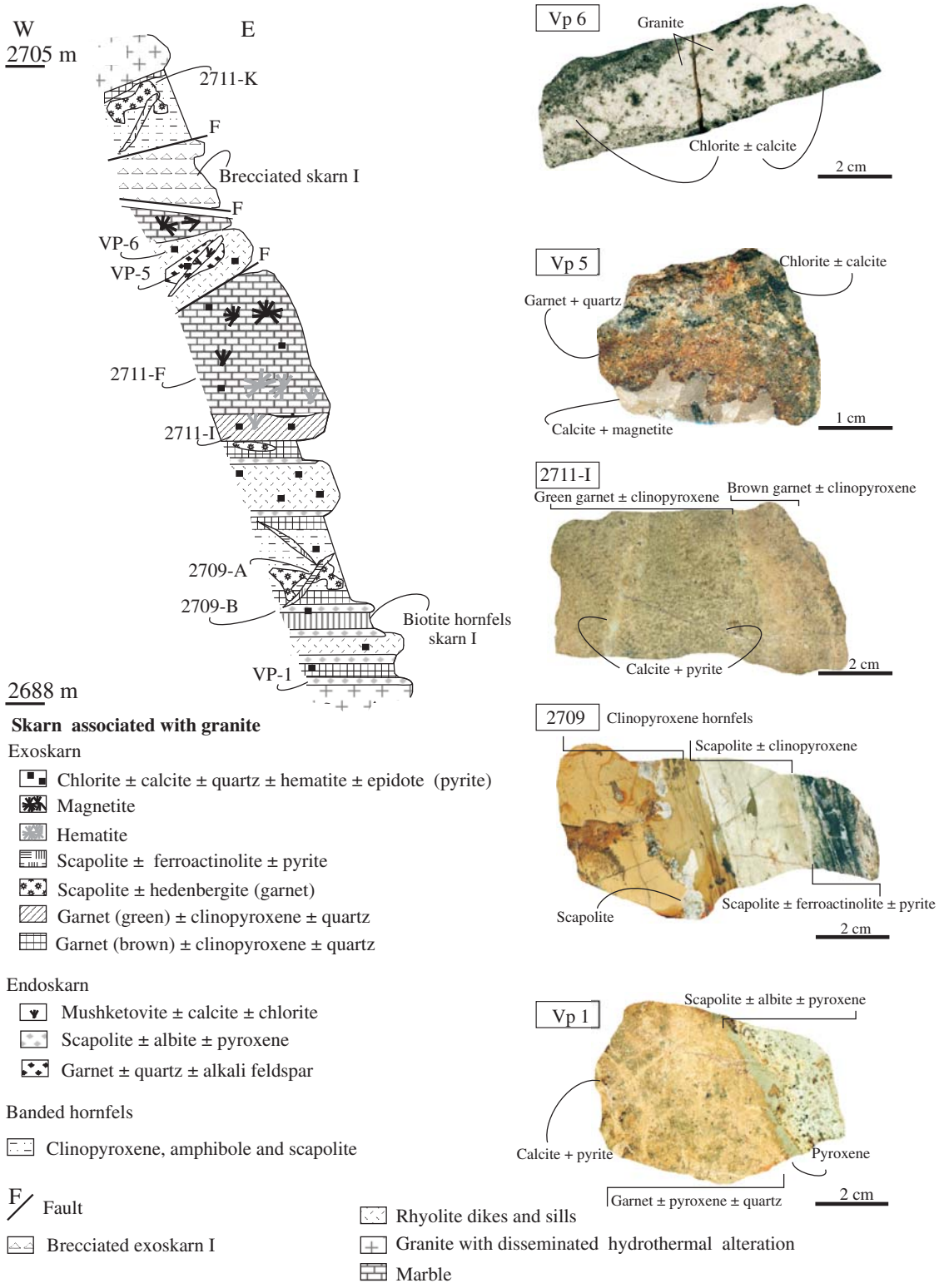

FIG. 12. Schematic east-west profile of the Fe skarn associated with granite and rhyolite, including photographs of the main alteration and mineralization styles in the profile. Sample Vp 6: chlorite ± calcite alteration of a rhyolite dike. Sample Vp 5: brown garnet ± quartz endoskarn partially altered to chlorite ± calcite and calcite ± magnetite-rich pockets. Sample 2711-I: contact between proximal brown garnet ± clinopyroxene and distal green garnet ± clinopyroxene exoskarn zones cut by late calcite ± pyrite veinlets. Sample 2709: scapolite ± clinopyroxene exoskarn in pyroxene hornfels cut by late scapolite ± ferroactinolite ± pyrite vein. Sample Vp 1: contact between the scapolite ± albite ± clinopyroxene endoskarn (rhyolite) and the brown garnet ± clinopyroxene ± quartz exoskarn with late calcite ± pyrite. A thin pyroxene envelope separates both zones.

TABLE 4. Representative Electron Microprobe Analyses of Scapolites from the Skarn Associated with Granite and Rhyolite

Sample no.	2709B-1		2709B-2	2709B-3	2709B-4	2709B-5	2709B-6	2709B-7	2709A-1	2709A-2	2709A-3	2709A-4	2709A-5	2709A-6
Location	Fig. 12				Fig. 12			Fig. 12						
(Wt %)														
SiO_2	56.58	55.93	57.23	56.61	56.58	56.18	56.49	56.08	55.93	56.95	58.41	58.52	58.04	56.65	57.51	55.19
TiO_2	n.d.	n.d.	n.d.	n.d.	0.01	n.d.	0.01	n.d.	0.03	0.05	0.03	0.06	0.01	n.d.	0.03	0.01	0.01
Al_2O_3	22.28	23.20	22.79	23.10	23.60	23.27	23.10	23.84	23.09	23.30	23.20	22.40	23.77	21.45	23.15	22.69	23.44
CaO	7.23	7.19	6.95	7.65	7.85	8.02	7.82	8.25	8.01	7.54	7.25	6.14	6.50	6.19	7.81	7.59	8.70
MgO	0.01	0.03	n.d.	n.d.	n.d.	n.d.	n.d.	n.d.	0.01	0.01	n.d.	n.d.	0.01	0.03	0.03	0.01	0.02
FeO	0.03	0.15	n.d.	n.d.	n.d.	n.d.	0.04	0.05	0.03	0.01	n.d.	0.01	0.10	0.12	0.04	0.14	0.10
MnO	0.02	0.09	n.d.	0.05	0.02	0.01	0.05	0.04	0.01	0.01	0.09	n.d.	0.07	0.12	0.04	n.d.	n.d.
K_2O	1.06	1.06	0.989	0.941	1.15	1.11	1.04	0.777	1.20	0.931	1.10	1.31	0.79	0.62	0.95	1.08	0.90
Na_2O	8.89	8.57	9.40	9.16	8.86	8.81	8.80	7.62	8.86	9.37	9.48	9.77	8.62	5.90	9.33	8.94	8.59
Total	96.11	96.20	97.36	97.50	98.08	97.40	97.35	96.65	97.17	98.17	98.09	98.16	98.56	92.50	98.12	98.04	96.98
Cations based on 25 oxygens																	
Si	8.34	8.24	8.32	8.24	8.19	8.20	8.24	8.20	8.19	8.23	8.25	8.42	8.36	8.69	8.22	8.32	8.11
Ti	0.00	0.00	0.00	0.00	0.00	0.00	0.00	0.00	0.00	0.01	0.00	0.01	0.00	0.00	0.00	0.00	0.00
Al	3.87	4.03	3.91	3.97	4.03	4.00	3.97	4.11	3.99	3.97	3.96	3.81	4.00	3.79	3.96	3.87	4.06
Ca	1.14	1.13	1.08	1.19	1.22	1.25	1.22	1.29	1.26	1.17	1.12	0.95	0.99	0.99	1.21	1.18	1.37
Mg	0.00	0.01	0.00	0.00	0.00	0.00	0.00	0.00	0.00	0.00	0.00	0.00	0.00	0.01	0.01	0.00	0.00
Fe^{2+}	0.00	0.02	0.00	0.00	0.00	0.00	0.01	0.01	0.00	0.00	0.00	0.00	0.01	0.01	0.00	0.02	0.01
Mn	0.00	0.01	0.00	0.01	0.00	0.00	0.01	0.00	0.00	0.00	0.01	0.00	0.01	0.02	0.00	0.00	0.00
K	0.20	0.20	0.18	0.17	0.21	0.21	0.19	0.14	0.22	0.17	0.20	0.24	0.14	0.12	0.18	0.20	0.17
Na	2.52	2.43	2.63	2.57	2.47	2.48	2.47	2.15	2.50	2.61	2.64	2.71	2.37	1.70	2.61	2.49	2.43
Meionite	29.71	30.77	27.77	30.43	31.28	31.89	31.65	36.25	31.75	29.74	28.56	24.45	28.78	36.10	30.72	30.80	34.80

n.d. = not detected

orthoclase + quartz alteration of diorite, but they are too small for microthermometric measurements. Fluid inclusions are well preserved in garnet, clinopyroxene, quartz, and calcite from the exoskarn associated with the diorite, but only fluid inclusions hosted in quartz from the clinopyroxene ± garnet ± quartz (feldspar) external veins of the exoskarn associated with granite were suitable for analysis.

Five types of fluid inclusions were identified based on their characteristics at room temperature (Nash, 1976): (I) two-phase, liquid-rich inclusions, (II) two-phase, vapor-rich inclusions, (III) three-phase inclusions, (IV) multi-solid-bearing inclusions, and (V) monophase vapor inclusions.

Fluid inclusions in igneous rocks

The interstitial quartz of the diorite, granodiorite, and granite has numerous planar arrays of secondary fluid inclusions along multiple healed fractures (Fig. 14). Along these trails saline fluid inclusions (types III and IV, with halite ± sylvite ± hematite ± $FeCl_n$) coexist with aqueous, vapor-rich fluid inclusions (type II, V >40%) and monophase vapor inclusions (type V).

Fluid inclusions in the skarn associated with diorite

In the inner exoskarn zone, garnet hosts primary and pseudosecondary, type II, III, IV, and V fluid inclusions. Most fluid inclusions have regular shapes, except for the vapor-rich (type II and V) inclusions, which have irregular and tubular shapes (Fig. 14). Solids identified in the three-phase and multisolid inclusions are halite, sylvite, and a reddish, slightly translucent opaque that is assumed to be hematite. These inclusions homogenized to a liquid (Th_L) at temperatures >550°C (Fig. 15A). Type IV fluid inclusions have salinities between 39 to 41wt percent NaCl equiv, based on Sterner et al. (1988) (Fig. 15B).

Quartz crystals of the inner exoskarn zone contain isolated primary and smaller pseudosecondary, type II, III, IV, and V fluid inclusions, and the most common solids are halite ± sylvite ± hematite (Fig. 14) and a tabular, light green and birefringent solid that could be $FeCl_n$ (cf. Shepherd et al., 1985). These inclusions homogenized to a liquid between 265° and 579°C (n = 18; Fig. 15A), by halite dissolution (T_m; n = 13) between 324° and >550°C, and by simultaneous halite dissolution and vapor disappearance (n = 2) at temperatures of 358° and 468°C. Only two type II fluid inclusions homogenized to a vapor at 575°C (Fig. 15A). The fluid inclusions have variable salinities between 39 to 67 wt % NaCl equiv (Fig. 15B). Secondary, type I fluid inclusions in quartz homogenized to a liquid between 148° and 288°C (Fig. 15A), and to a vapor at 280° and 320°C (Fig. 15A).

In the intermediate (garnet ± clinopyroxene) zone of the exoskarn, the isotropic garnet cores contain abundant primary fluid inclusions. They are types II, III, IV, and V inclusions with ovoid and irregular shapes (Fig. 14). The type IV inclusions are more abundant, and solids comprise more than 50 percent of the inclusion volume. The fluid inclusions hosted in pyroxene are primary, with regular shapes, contain multiple solids (type IV) or are monophase (V) (Fig. 14). Identified solids in fluid inclusions in both calc-silicates are halite ± sylvite ± $FeCl_n$ ± hematite. Most fluid inclusions in pyroxene and garnet homogenized to a liquid by halite dissolution (T_m)

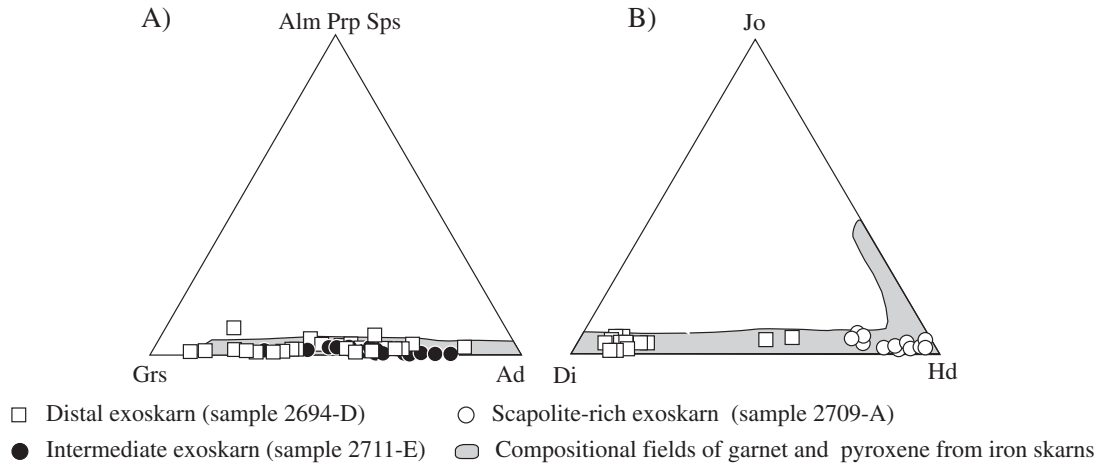

FIG. 13. A. Composition of garnet from the Vegas Peladas exoskarns associated with granite (sample 2711-I, Fig. 12; sample 2694, Fig. 3B). B. Composition of pyroxene from the Vegas Peladas exoskarns associated granite (samples 2711-I and 2709-A, Fig. 12; sample 2694, Fig. 3B). The compositional fields for garnet and pyroxene in Fe skarn deposits (Meinert et al., 2005) are shown in both diagrams for comparison. Ad = andradite, Alm = almandine, Di = diopside, Grs = grossular, Hd = hedenbergite, Jo = johannsenite, Prp = pyrope, Sps = spessartine.

and by vapor bubble disappearance (Th_L) at temperatures higher than 500°C, similar to the fluid inclusions in garnet from the inner garnet zone, but their salinities are higher (38–67 wt % NaCl equiv: Fig. 15C, D). A group of seven fluid inclusions in garnet homogenized by disappearance of the vapor bubble at lower Th (304° to 400°C) and has salinities between 38 and 42 wt % NaCl equiv (Fig. 15C, D). Secondary, type I fluid inclusions in garnet homogenized at lower temperatures (180°–268°C) and have lower salinities (7.8 to 23 wt % NaCl equiv, n = 6: Fig. 15C, D) than the primary fluid inclusions. Their eutectic temperatures (–34° to –38°C) suggest that these fluids belong to a chemically complex system such as mixed H_2O-$FeCl_2$ (Te: –35°C), H_2O-NaCl-$FeCl_2$ (Te: –37°C) and H_2O-Na_2CO_3-K_2CO_3 (Te: –37°C) (cf. Borisenko, 1977).

In the external garnet ± clinopyroxene veins, garnet hosts primary type III fluid inclusions with halite daughter crystals and pseudosecondary two-phase types I and II inclusions. The primary fluid inclusions homogenized to a liquid by vapor disappearance at >550°C and have salinities between 33 and 34 wt % NaCl equiv (Fig. 15C, D), whereas the pseudosecondary fluid inclusions have lower salinity (19.5 wt % NaCl) and homogenization temperatures (216°–400°C). The eutectic melting temperatures of these pseudosecondary fluid inclusions were variable (–40°, –48°, and –52°C), suggesting similar chemically complex fluids as in garnet from the intermediate zone, but with addition of $MgCl_2$ and higher $CaCl_2$ (cf. Borisenko, 1977; Crawford, 1981).

In the retrograde epidote + hematite (partly replaced by magnetite) + quartz assemblage that replaces the intermediate exoskarn zone, the quartz contains numerous fluid inclusions of types I, II, III, and IV (Fig. 14), with halite ± sylvite and less common $FeCl_n$ ± $CO_3^=$ solids. In contact with magnetite after hematite, quartz hosts fluid inclusion trails aligned along with opaque (hematite-magnetite?) microinclusions. Measured homogenization temperatures (Th_L) and salinities from these inclusions were 215° to 436°C and 24.3 to 48.5 wt % NaCl equiv (Fig. 15E, F). In the saturated fluid inclusions, the dissolution temperatures of daughter crystals were lower than the homogenization temperatures. Six type II fluid inclusions associated with saturated fluid inclusions homogenized to a vapor at similar temperatures (320° and 420°C) (Fig. 15E). The eutectic temperatures (ET) measured in the two-phase fluid inclusions (–43 and –55°C) indicate a chemically complex fluid with H_2O-$CaCl_2$-KCl (with a theoretical eutectic at –50.5°C: cf. Borisenko, 1977), H_2O-$CaCl_2$ (with a theoretical eutectic at -49.8°C: cf. Borisenko, 1977) and other salts (NaCl, $FeCl_2$ and Na_2CO_3) in variable proportions.

In this external zone of the exoskarn, the interstitial calcite and calcite in veinlets that cut garnet, clinopyroxene, and amphibole contain primary, two-phase fluid inclusions with triangular and regular shapes (Fig. 14). These fluid inclusions have homogenization temperatures between 165° and 315°C (Fig. 15G) and the lowest salinities (8.4-13.51 wt % NaCl equiv; Fig. 15H) measured in the system. The eutectic temperatures vary between -15° to -35°C, indicating the presence of NaCl-H_2O and KCl with variable proportions of $MgCl_2$ and $FeCl_2$.

Fluid inclusions in the skarn associated with granite

In the inner zone of the exoskarn, clinopyroxene contains primary saline and vapor-rich fluid inclusions, but they are too small to be analyzed. Quartz from the external veins of the exoskarn contains excellent primary and pseudosecondary type III, IV and V fluid inclusions, with halite ± opaque (sylvite) and less common, two-phase type II fluid inclusions. The type III and IV fluid inclusions homogenized to liquid at temperatures higher than the dissolution temperatures of daughter crystals (289° to >550°C; Fig. 15I). They have variable salinities between 30.3 and 45.3 wt % NaCl equiv (Fig. 15J). The type II fluid inclusions homogenized to a liquid between 469° and >550°C (Fig. 15I). Two vapor-rich fluid inclusions associated with the saturated fluid inclusions homogenized to a vapor at ~ 450°C, and another two, at ~550°C (Fig. 15I). Based on the solids present in the

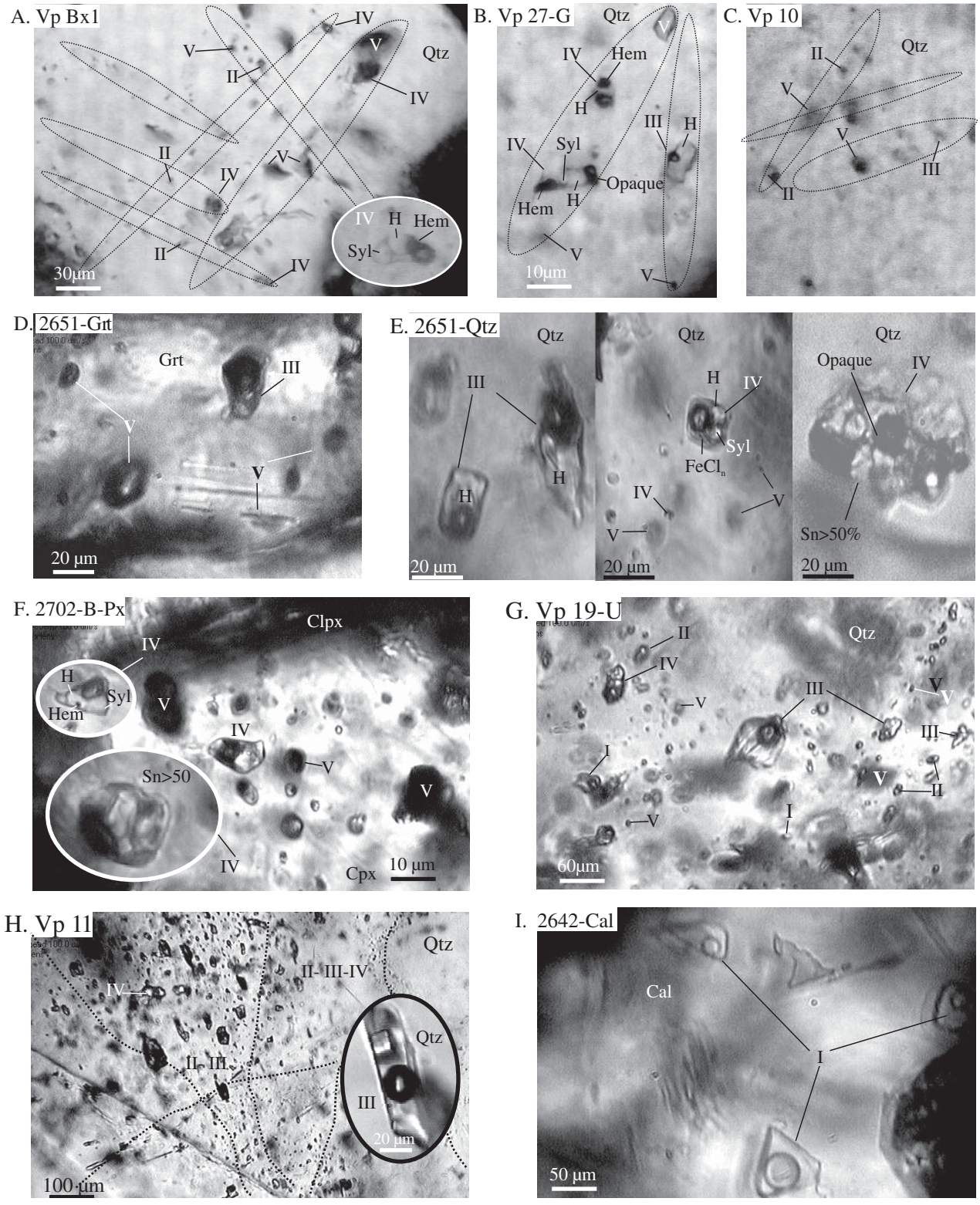

FIG. 14. Photomicrographs of fluid inclusions hosted in quartz crystals from (A) diorite xenolith—sample Vp Bx1; Fig. 3A; (B) granodiorite—sample Vp 27-G; Fig. 3A; and (C) granite (sample Vp 10; Fig. 3A). (D) Fluid inclusions hosted in garnet—sample 2651-Grt; Fig. 7; and (E) in quartz—sample 2651-Qtz, Fig. 7, from the inner exoskarn zone associated with diorite. (F, G) Fluid inclusions hosted in quartz (sample Vp19U, Fig. 8; sample Vp11, Fig 3B) from the intermediate exoskarn zone and (H) in late calcite—sample 2642; Fig. 6, from the external zone. Cal = calcite, Clpx = clinopyroxene, Grt = garnet, H = halite, Hem = hematite, Qtz = quartz, Sn = multiple solids, Syl = sylvite. I = two-phase, liquid-rich fluid inclusions, II = two-phase, vapor-rich inclusions, III = three-phase inclusions, IV = multi-solid-bearing inclusions, V = monophase vapor inclusions.

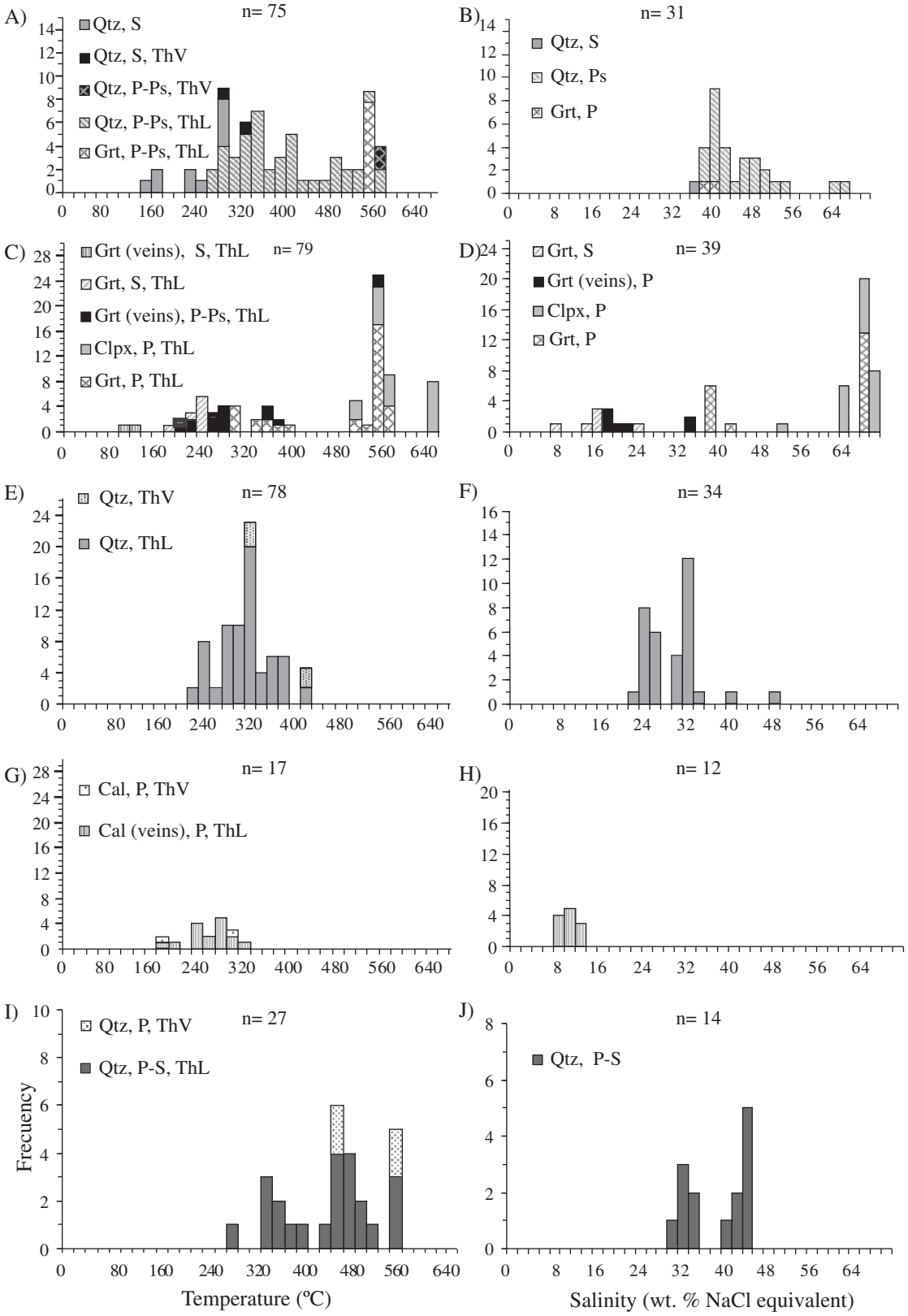

FIG. 15. Histograms summarizing calc-silicate, quartz, and calcite-hosted fluid inclusion homogenization temperatures and salinities from the Vegas Peladas skarns associated with diorite (A to H) and granite (I and J). Cal = calcite, Clpx = clinopyroxene, Grt = garnet, L = liquid, n = number of measured fluid inclusions, P = Primary, Ps = pseudosecondary, Qtz = quartz, S = secondary, Th = homogenization temperature, V = vapor.

saturated fluid inclusions, these fluids belong to the H_2O-NaCl- $FeCl_2$ system.

Pressure determination

In iron skarn associated with diorite, the presence of saline fluid inclusions in the quartz of the retrograde alteration (epidote + hematite or magnetite) associated with vapor-rich fluid inclusions, which homogenized at similar temperatures (320° and 420°C), suggests boiling during the formation of the quartz. The temperatures and salinities of the boiling fluids were between 320° and 420ºC and 24.3 and 41.6 wt % NaCl equiv, respectively, corresponding to vapor pressures of 125 and 325 bars (Zhang and Frantz, 1987). The maximum hydrostatic pressure for boiling fluids corresponds to depths of at least 3.5 km. For fluid inclusions with evidence of boiling, it is most likely that the fluids were trapped in growing minerals on the liquid-vapor curve and, thus, the homogenization temperature is equal to the trapping temperature. However, evidence for boiling was not found in other prograde silicate minerals (garnet and pyroxene), suggesting that lithostatic pressures may have prevailed in the initial stages of skarn formation. For these early, nonhydrostatic conditions, 3.5 km of rocks with an average density of 2.7 g/cm^3 corresponds to a lithostatic pressure of approximately 1 kbar.

In skarn associated with granite, the presence of multisolid inclusions (with 41 wt % NaCl equiv) and vapor-rich inclusions hosted in the quartz of the external veins with similar high homogenization (to liquid and to vapor) temperatures (~450° and ~550°C) also probably indicates immiscibility (Shepherd et al., 1985). Thus, these temperatures could be interpreted as the fluid trapping temperature, corresponding to a hydrostatic pressure of 450 bars.

Stable Isotopes

The $\delta^{18}O$ values were determined on 18 minerals from the iron skarn associated with diorite and in biotite and plagioclase from the diorite pluton (sample 2685, Table 5). The δD values were determined for epidote from the endoskarn associated with diorite (sample 2653-C). $\delta^{13}C$ values were measured in calcite from the latest stage of retrograde alteration (sample 2692) and in marble (sample 2711-F). The results are summarized in Table 5. Garnet from the inner and intermediate exoskarn zone was not analyzed owing to its numerous poikilitic inclusions.

Water composition and thermometry

Calculated values reported in Table 5 were obtained applying published fractionation factors. The equilibrium isotopic temperature calculated for the plagioclase-biotite pair in the diorite was ~638°C. Temperatures calculated for the epidote-magnetite pairs from the retrograde alteration of the exoskarn zones are 569° to 634°C. These temperatures are unreasonably high, consistent with these assemblages replacing the prograde minerals of the exoskarn, indicating that they were not deposited as an equilibrium assemblage. Temperatures for the calcite-epidote mineral pair could not be determined because of the lack of experimentally determined fractionation factors for this mineral pair.

The temperature ranges obtained from fluid inclusion analyses, combined with the temperatures calculated using the isotopic composition of mineral pairs, were used to constrain the isotopic compositions of coexisting fluids (Table 5). The temperature of formation used for the magnetite, epidote, and quartz alteration of the inner exoskarn zone and for the epidote of the endoskarn was estimated, combining the temperatures of the fluid inclusion data from quartz (garnet ± quartz zone) and the lower T limit for andradite stability in similar skarn environments (380°–450°C: Bowman, 1998). Minimum temperatures of formation of the amphibole-rich retrograde alteration were assumed to be similar to the homogenization temperatures of secondary fluid inclusions in the garnet (180°–268°C), since they replace the garnet ± clinopyroxene veins of the external exoskarn zone and hornfels. The homogenization temperature range (165°–315°C) of fluid inclusions in calcite was used for epidote from the latest retrograde assemblage. Fluid inclusion data for calcite from the marble were not available, so we used the homogenization temperatures obtained for fluid inclusions in garnet and clinopyroxene from the prograde exoskarn (580°–670°C).

The $\delta^{18}O_{H_2O}$ values in equilibrium with the quartz and epidote alteration of the diorite are 6.2 to 7.1 per mil and –0.2 to +3.8 per mil, respectively. The δD_{H_2O} of the fluids in equilibrium with epidote from the endoskarn are –51.9 to –44.1 per mil. For the fluid in equilibrium with garnet, the $\delta^{18}O_{H_2O}$ of the fluid is 7.23 to 8.5 per mil. For the fluids in equilibrium with the epidote + magnetite ± quartz from the inner zone of the exoskarn, $\delta^{18}O_{H_2O}$ values are 2.77 to 3.57 per mil for epidote, 3.29 to 4.52 per mil for quartz, and 4.81 to 7.98 per mil for magnetite. The $\delta^{18}O_{H_2O}$ values of fluid in equilibrium with the retrograde amphibole from the external veins are 4.57 to 6.69 per mil for ferropargasite and –0.55 to +3.67 per mil for the actinolite. For the fluids in equilibrium with the latest retrograde minerals, $\delta^{18}O_{H_2O}$ values are –4.7 to +0.7 per mil for epidote and –3.9 to +2.7 per mil for calcite. The $\delta^{13}C$ value of the C (CO_2 or HCO_3^-?) in the fluid in equilibrium with this calcite is –10.3 to –7.2 per mil. For fluids in equilibrium with the marble the respective $\delta^{18}O_{H_2O}$ and $\delta^{13}C$ values are 9.96 to 10.5 per mil and –9.9 to –10.1 per mil.

Discussion

Two metasomatic events have been identified in the Vegas Peladas district associated with two of the four igneous rock types that intrude the Jurassic sedimentary rocks of the area. Contact metamorphism and metasomatism resulted in the transformation of sedimentary and igneous rocks into hornfels, marble, and skarn, and each of the mineralized skarns has distinctive characteristics that reflect differences in hydrothermal fluid composition and source.

Geology and alteration

The skarn associated with the diorite pluton contains garnet and subordinate clinopyroxene as prograde calc-silicates in the exoskarn zones. The chemical compositions of garnet show an increase in iron from inner ($And_{31–89}$ $Py_{0.3–2}$) to external zones ($And_{92–100}$ $Py_{0–0.1}$). This is also manifested at the scale of some individual garnet crystals, with an increase in the andradite content from core (Ad_{45} $Py_{0.88}$) to rim (Ad_{100} Py_0). Clinopyroxene has a wide compositional range ($Di_{24–70}$ $Jo_{1–4}$). The hydrous silicates (epidote and amphibole) with quartz and albite replace the prograde calc-silicates. Epidote

TABLE 5. Stable Isotope Results (H, C, O) Determined in Minerals Separated from the Diorite Pluton, and from the Alterations Associated with the Diorite

			Mineral values				Estimated temperature °C		1000 ln $\alpha_{\text{Mineral-fluid}}$						Fluid values							
									$^{18}O_{SMOW}$ T°		D_{SMOW} T°		$^{13}C_{PDB}$ T°		$^{18}O_{SMOW}$ T°		D_{SMOW} T°		$^{13}C_{PDB}$ T°			
Sample no.	Location	Mineral	$\delta^{18}O_{SMOW}$	δD_{SMOW}	$\delta^{13}C_{PDB}$	$\delta^{18}O_{PDB}$	Min	Max	Min	Max	Min	Max	Min	Max	Min	Max	Min	Max	Min	Max	Calculated T°C	Reference[1]
2685	Fig. 3A	Plg	6.90						–1.3						8.20						638	Zheng (1993a)
2685	Fig. 3A	Bt	5.40						–2.5						7.93						638	Zheng (1993b)
2653-C	Fig. 7	Qtz	8.30				580	670	2.11	1.2					6.19	7.10						Sharp and Kirschner (1994)
2653-C	Fig.7	Ep	2.80				380	450	–0.2	–0.8					2.97	3.57						Zheng (1993b)
2653-C	Fig. 7	Ep	3.10	–92			380	450	–0.2	–0.8	–40	–44			3.27	3.87	–51.9	–47.9				Zheng (1993b); Graham et al. (1980); Chacko et al. (1999)
2711-F	Fig. 12	Cal	11.728		–12.504	–18.606	580	670	1.76	1.28			–2.6	–2.4	9.968	10.45			–9.864	–10.1		Zheng (1999); Ohmoto and Rye (1979); Bottinga (1969)
2642	Fig. 6	Parg	5.6				180	268	1.03	–1.1					4.57	6.69						Zheng (1993b)
2656-2	Fig. 7	Act	4.5				180	268	3.45	0.83					1.05	3.67						Zheng (1993b)
2656-2	Fig. 7	Act	4.5				180	268	3.45	0.83					1.05	3.67						Zheng (1993b)
2656-1	Fig. 7	Act	2.9				180	268	3.45	0.83					–0.55	2.07						Zheng (1993b)
2684	Fig. 6	Ep	2.8				380	450	–0.2	–0.8					2.97	3.57					634–569	Zheng (1993b)
2684	Fig. 6	Ep	2.6				380	450	–0.2	–0.8					2.77	3.37					634–569	Zheng (1993b)
2684	Fig. 6	Mt	–2.7				380	450	–8	–7.5					5.28	4.81					634–569	Cole et al. (2004); Zheng (1991); Zheng and Simon (1991)
2692	Fig. 3B	Grt	5.6				216	550	–1.6	–2.9					7.23	8.53						Zheng (1993a)
2692	Fig. 3B	Grt	5.6				216	550	–1.6	–2.9					7.23	8.53						Zheng (1993a)
2692	Fig. 3B	Ep	0.9				165	315	5.56	0.72					–4.66	0.18						Zheng (1993b)
2692	Fig. 3B	Ep	1.4				165	315	5.56	0.72					–4.16	0.68						Zheng (1993b)
2692	Fig. 3B	Cal	8.058		–9.332	–22.166	165	315	12	5.38			0.92	–2.2	–3.90	2.68			–10.25	–7.17		Zheng (1999); Ohmoto and Rye (1979); Bottinga (1969)
2702	Fig. 3B	Mt	0				380	450	–8	–7.5					7.98	7.51						Cole et al. (2004); Zheng (1991); Zheng and Simon (1991)
2704-C	Fig. 3B	Qtz	8.2				380	450	4.91	3.68					3.29	4.52						Zheng (1993a)

[1] The isotopic values of the fluids in equilibrium with the analyzed minerals have been calculated using the fractionation factors of the authors; abbreviations: Act = actinolite, Bt = biotite, Cal = calcite, Ep = epidote, Grt = garnet, Mt = magnetite, Parg = pargasite, Plg = plagioclase, Py = pyrite, Qtz = quartz

(rich in Al and Fe) is abundant in the inner and intermediate exoskarn zones; it also dominates in the endoskarn. Amphibole occurs in both the endoskarn and in the exoskarn, but it is abundant in the external exoskarn zone. Actinolite that forms a selvage on the iron oxide veins that cut the hornfels has Ca, Ti, and Al concentrations similar to the secondary amphibole in the diorite, but higher iron concentration. The ferropargasite that replaces the hedenbergitic clinopyroxene veins from the external exoskarn zone has the highest Ti, Al, and Fe concentrations of all amphiboles. These compositional variations are interpreted to reflect local fluctuations of the hydrothermal fluid composition that reacted with the wall rock (Hemley and Hunt, 1992). The positive Eu anomalies in the retrograde assemblages with magnetite and hematite and the increase of hematite relative to magnetite from inner to outer zones indicate high oxygen fugacity during the retrograde stage (Rollinson, 1993).

The skarn associated with the granite pluton is rich in garnet and clinopyroxene replacing marble and scapolite, clinopyroxene, garnet, and alkali feldspar replacing hornfels. Where skarn is developed in marble, the garnet ($Ad_{10–83}$) and clinopyroxene ($Di_{82–100}$) in the intermediate and distal exoskarn zones are richer in Al and Mg than garnet and clinopyroxene from equivalent exoskarn zones associated with diorite. Only clinopyroxene that replaces hornfels with scapolite (garnet ± pyrite), has high Fe ($Hd_{74–94}$) due to reduction (lower oxygen fugacity) of the hydrothermal fluids caused by reaction with the more reduced wall rock (hornfels) (Franchini et al., 2000). The scapolite ($Me_{25–36}$) ± ferroactinolite ± pyrite assemblage replaces and cuts previous alterations and marks the beginning of retrograde stage.

Fluid chemistry

The characteristics of the hydrothermal fluids that formed the different skarn zones associated with the diorite pluton are summarized in Figure 16A.The association of primary multisolid and vapor-rich fluid inclusions in quartz of the diorite and in silicates of the prograde exoskarn is interpreted to have been a result of unmixing of a magmatic fluid of low to moderate salinity (6–8 wt % NaCl equiv) that exsolved from the diorite into a brine and a vapor of low density (Fig. 16B; e.g., Burnham, 1979; Bodnar et al., 1985; Cline and Bodnar, 1991; Yang and Bodnar, 1994; Bordnar, 1995). This unmixing occurred when the initial hydrothermal fluids were exsolved from the diorite at 3.5 km depth, at temperatures of ~670°C, and lithostatic pressures of ~1 kbar.

Fluid inclusions in the inner and intermediate exoskarn zones define three populations based on homogenization by vapor disappearance (Th), by halite dissolution (Tm) or simultaneous halite-vapor disappearance (Th = Tm). Experimental

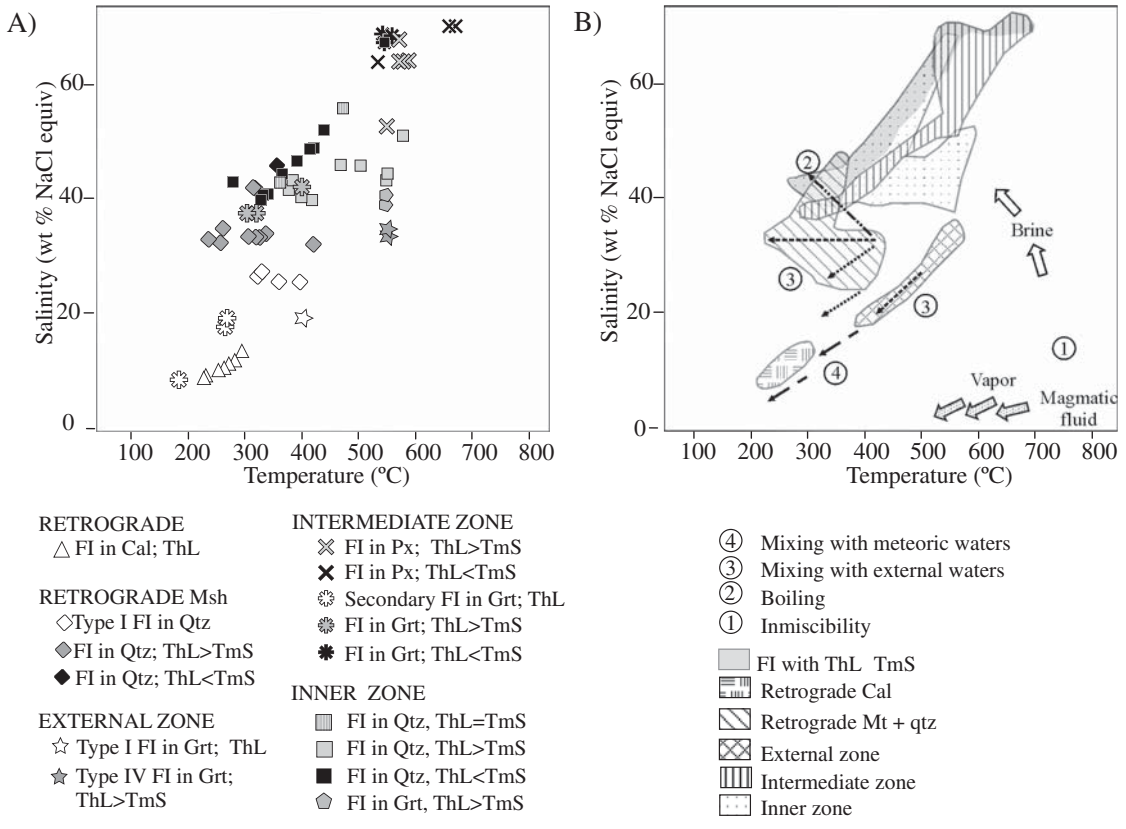

FIG. 16. A) Plot of fluid inclusion homogenization temperature vs. salinity from the Fe skarn associated with diorite. B) Similar diagram of A although the numbers 1 to 4 indicate the different physicochemical processes and changes of temperature and pressure occurred during the evolution of the hydrothermal system. Hypothetical conditions (temperature and salinity) of the initial exsolved magmatic fluids are also represented. Cal = calcite, FI = fluid inclusions, Grt = garnet, Mt = magnetite, P = pressure, Px = pyroxene, Qtz = quartz, T = temperature, ThL = homogenization temperature to liquid, TmS = homogenization temperature by halite dissolution; FI = fluid inclusion.

work (Cline and Bodnar, 1994, p. 1795) suggests that saline fluid inclusions that homogenize by halite dissolution or by simultaneous halite-vapor disappearance may have been trapped as immiscible saline fluids, and this may have occurred during the formation of the Vegas Peladas iron skarn (Fig. 16B). The calculated $\delta^{18}O$ values of waters in equilibrium with garnet (7.2–8.5‰) and with magnetite (4.8–7.98‰) are similar to the $\delta^{18}O$ values of the magmatic fluids (Fig. 17; Taylor, 1986; Meinert et al., 2003). Some of the fluid inclusions in the garnet of the external garnet ± clinopyroxene veins also have homogenization temperatures and salinities similar to fluid inclusions of the inner and intermediate prograde exoskarn minerals (Fig. 16B).

The population of fluid inclusions hosted in the retrograde quartz associated with the iron oxides from the intermediate exoskarn zone recorded both boiling with decreasing temperatures and increasing salinities and mixing with external fluids with a decrease in temperature and salinity (Fig. 16B). These fluid inclusions have carbonate daughter minerals in addition to some of the salts present in the fluid inclusions of earlier silicate minerals.

The $\delta^{18}O_{H_2O}$ values (4.57–6.69‰) of the fluid in equilibrium with ferropargasite that replaces the clinopyroxene are intermediate between the values obtained for the prograde and retrograde minerals (Fig. 17). The general trend toward lower $\delta^{18}O$ values of the fluid in equilibrium with the retrograde epidote (2.8–3.57‰), quartz (3.29–4.52‰) and actinolite (–0.55 to +3.67‰), suggests a decrease in temperature after boiling and/or partial mixing of hydrothermal fluids with another fluid of meteoric derivation. Gradual dilution of the magmatic fluid by meteoric water is also suggested by the low total REE concentration in the epidote-and amphibole-rich alteration compared to the prograde exoskarn assemblages (cf. Taylor, 1986).

Another population of saline aqueous fluid inclusions in the garnet of the external garnet ± clinopyroxene veins has lower homogenization temperatures and salinities (Fig. 16A), and has a different chemical composition ($CaCl_2$ and possibly $MgCl_2$ in addition to $FeCl_2$ and other salts). These fluid inclusions are aligned in a trend with the fluid inclusion population in late, retrograde calcite which have the lowest homogenization temperatures (165°–315°C) and salinities (8.41–13.51 wt % NaCl equiv) (Fig. 16B). The $\delta^{18}O$ values of the water in equilibrium with this late epidote (–4.66 to –0.19‰) and calcite (–3.9 to –2.68‰) suggest mixing and dilution of the magmatic fluids with meteoric water (with predominance of the later; Fig. 17) during the collapse of the hydrothermal system (cf. Bowman, 1998; Fournier, 1999; Meinert et al., 2005).

The $\delta^{18}O$ (9.98–10.45‰) and $\delta^{13}C$ (–9.86 to –10‰) values of the fluids in equilibrium with calcite from the marble are lower than the values of fluids in equilibrium with a marine limestone ($\delta^{18}O$ >21‰ and $\delta^{13}C$ >1‰) (Fig. 17). This could

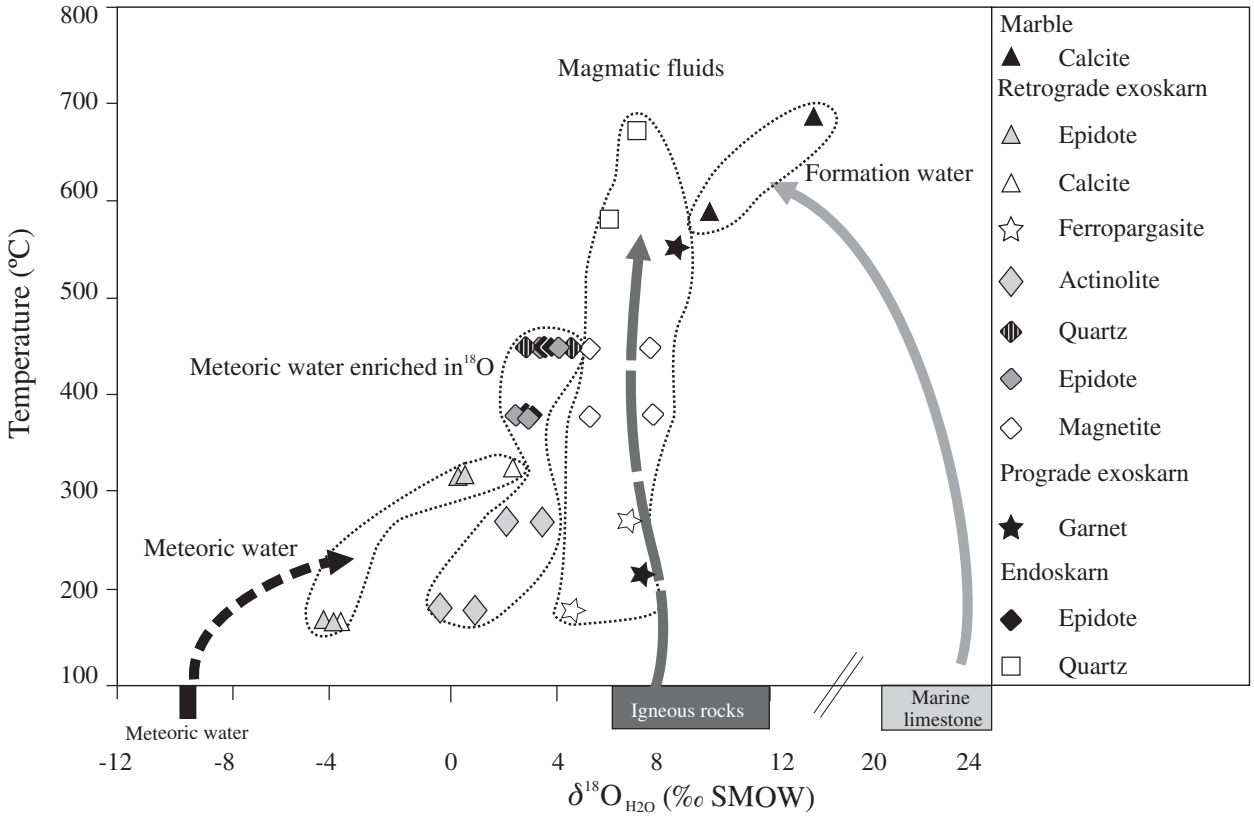

FIG. 17. Temperatures versus $\delta^{18}O$ values of waters in equilibrium with minerals from the Fe skarn associated with diorite. The fields group minerals with similar isotopic signature. The arrows represent different sources of fluid involved in the formation of the minerals: dark gray line comprising long dashes = magmatic fluids; continuous gray line = formation fluids, and gray line comprising short dashes = meteoric water. The fields of $\delta^{18}O$ magmatic and carbonates marine rocks are from Taylor, 1986.

reflect isotopic exchange between calcite and graphite present in the Calabozo Formation (Dessanti, 1978) during the thermal metamorphism (Bowman, 1998) or between the host rock and magmatic fluids with significantly different ^{18}O concentration (Bowman, 1998).

Iron mineralization

The presence of hematite and $FeCl_n$ in the early, high-temperature (homogenization temperatures up to 670°C), and high salinity fluids (up to ~70 wt % NaCl equiv) indicates that these fluids were capable of transporting abundant iron in solution (Hemley et al., 1992; Hemley and Hunt, 1992). In contrast, the fluid inclusions in quartz associated with the iron ore indicate boiling, lower temperature (320° and 420°C), and lower salinity (23–41.6 wt % NaCl equiv) fluids at hydrostatic pressures (125 and 325 bars). Experiments on Fe solubility under these conditions (Whitney et al., 1985; Hemley et al., 1992, Simon et al., 2004) indicate that a decrease in temperature from 670°C to the boiling temperatures (420°–320°C) and salinity (67–24 wt % NaCl equiv) documented for the Vegas Peladas skarn system would cause a notable decrease in iron solubility despite the declining pressure.

Comparison with other Fe skarns

Skarns in the Vegas Peladas district are similar to other Fe skarn deposits worldwide (Einaudi et al., 1981; Meinert, 1984; Zhao et al., 1990; Zürcher et al., 2001; Foster et al., 2004; Meinert et al., 2005) and to other iron skarns located in the same belt of southwest Mendoza (Franchini and Dawson, 1999; Franchini et al., 2005): (1) they are associated with primitive intrusions, (2) the skarns are zoned in space and time, (3) the prograde exoskarn zones are rich in andradite-grossularite garnet, diopside-hedenbergite pyroxene, and retrograde amphibole, epidote, quartz, chlorite, and calcite, (4) magnetite and hematite are the main iron ore minerals, and the most important orebodies are associated with retrograde mineral assemblages, (5) sulfides, mainly pyrite, are scarce (1 vol %) and occur in the endoskarn and distal zones, (6) the distribution of alteration and mineralization during early, prograde stages was strongly influenced by the composition of the host rocks (both igneous and sedimentary), whereas late, retrograde alteration was more strongly controlled by structure, (7) early, high-salinity fluids contained large amounts of Fe in solution.

However, several features of the Vegas Peladas skarns differ from other Fe skarns: (1) they were formed in a Miocene magmatic arc environment of an active continental margin, (2) endoskarn is poorly developed, (3) they contain orthoclase as an alteration product of the diorite, (4) Na metasomatism and scapolitization does not correlate with the highest iron ore grades, and (5) the total resource is lower than most of the Fe skarns worldwide (<10 Mt), possibly owing to the present erosion level of the hydrothermal system (Fig. 18A).

Conclusions

The geologic and geochemical characteristics of the Vegas Peladas Fe skarn deposit are typical of the Fe skarns in the Mendoza region of Argentina. The deposit formed by the overprinting and juxtaposition of two different metasomatic events associated with two different Miocene calc-alkaline plutons that intruded the Jurassic sedimentary rocks as illustrated in Figure 18. At a depth of ~3.5 km and lithostatic pressures of 1 kbar, high-temperature (~670°C) and low- to moderate-salinity (6–8 wt % NaCl equiv), magmatic fluids exsolved from the diorite pluton and separated into a dense, NaCl ± KCl ± $FeCl_n$ saline fluid and a low density vapor. These early hydrothermal fluids flowed up and outward from the igneous body and reacted with the metasedimentary host rocks to form the prograde exoskarn with disseminated magnetite (670°–400°C). Continued fluid exsolution from the magma and the sealing of fluid flow conduits by early silicate minerals exceeded lithostatic pressures, thus fracturing the rocks and causing boiling and further fracturing. This permitted the entry of external fluids into the hydrothermal system. The resulting mixed fluids cooled (420° to <320°C), causing the replacement of the early exoskarn silicates by hydrated minerals, quartz, and iron oxides. The fluids continued cooling below 320°C and the proportion of meteoric water increased gradually, generating the later and distal retrograde assemblages rich in calcite, epidote, and chlorite with scarce pyrite. The temperature and salinity decrease of the hydrothermal fluids was the main cause of massive iron precipitation. The early diorite-related skarn system was followed by intrusion of the granite pluton which reheated the wall rock to >550°C and also generated saline + vapor fluids by immiscibility that were capable of redistributing some of the iron from the preexisting skarn.

The Vegas Peladas Fe skarn is similar to the many other calcic Fe skarns that have been described in the literature. The multiple intrusive events produced a slightly more complicated deposit, but the mineral assemblages and hydrothermal processes are similar to those documented elsewhere. New dating (Franchini et al., 2007) and the present study demonstrate that the iron skarns of southwest Mendoza are associated with the least differentiated plutons, dikes, and sills of the voluminous and ubiquitous magmatism of the Upper Miocene. These Neogene igneous rocks were derived from primitive magmas that originated in the mantle, with little to no crustal contamination. These plutons occur at the intersection of the main lineaments, thrusts, and fold cores in poorly explored areas, and may host potentially significant iron mineralization in associated skarn. The distribution of alteration assemblages observed in Vegas Peladas can be used in these poorly explored areas as a guide to skarn mineralization.

Acknowledgments

This work forms part of a project financed by CONICET (PIP Nº 2726) and a Student Research Grant awarded by SEG (Society of Economic Geologists). We express our appreciation to Graciela Mas and Leandro Bengochea (CONICET-U. N. del Sur, Bahía Blanca) for their collaboration in the fluid inclusion study of the Vegas Peladas Fe skarn, Colombo Tassinari (CPGeo- Geosciences Institute, San Pablo University, Brazil) and Sol O´Leary (CONICET- U. N. del Comahue) for their collaboration in obtaining isotopic ages, Karina Mykietiuk (INREMI, U. N. de La Plata), Agustín Martín Izard (Departamento de Geología at the U. de Oviedo, Spain) for the microprobe analyses, Agnes Impiccini (CIMAR, U.N. del Comahue) for X-ray analyses and to Diego T. Licitra (Repsol-YPF), Raúl de Barrio, Mabel Lanfranchini, and Mauricio González Guillot (CONICET-INREMI, U. N. de La Plata) for their help in the field work. We thank D.

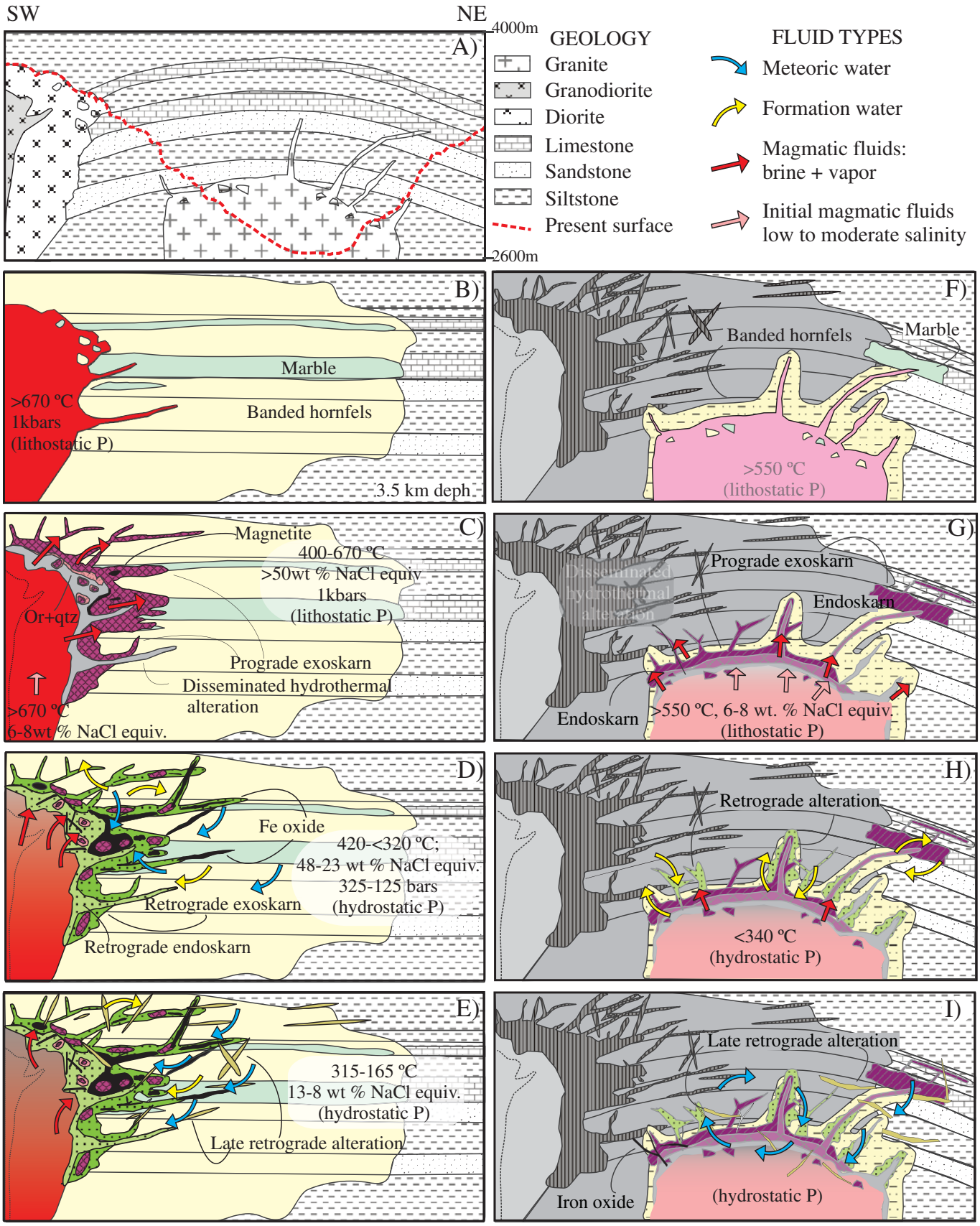

FIG. 18. Schematic representation of the evolution of the hydrothermal system, including formation of the iron skarn associated with diorite (A-E) and the skarn associated with granite (F-I).

Lentz, Fernando Tornos, and an anonymous reviewer for their helpful and constructive reviews which led to further improvement of the manuscript. Late editorial revision by M. Hannington is gratefully acknowledged.

May 16, 2008; February 2, 2009

REFERENCES

Angelelli, V., 1942, El yacimiento de calcopirita del cerro La Virgen. Los depósitos de magnetita y hematina de Vegas Peladas y los de Baritina y mineral manganesífero del arroyo Las Minas. Distrito de Malargüe, Departamento de San Rafael: Buenos Aires, Dirección de Minas y Geología, File (carpeta) 101, 17 p. (4 sheets).

Arrospide, A., 1972, Depósitos de minerales de hierro de Vegas Peladas Mina "Nenche", dpto. de Malargüe, Mendoza, República Argentina: Revista de la Asociación Argentina de Mineralogía, Petrología y Sedimentología, v. 3, p. 117–131.

Baldauf, P.G., Stephens, G.M., Kunk, M., and Nullo, F., 1992, Argon-Argon ages for the Huincán intrusive suite and their implications for the structural development of the Andean foreland, Southern Mendoza province, Argentina [abs.]: Geological Society of America, Abstract with Programs 24, A188.

Bellieni, G., Visentin E.J., and Zanettin B., 1996, Use of chemical TAS diagram (total alkali silica) for classification of plutonic rocks: Problems and suggestions: I.U.G.S.: Subcommission on the Systematics of Igneous Rocks Contribution no. 157, 35 p.

Bodnar, R.J., 1995, Fluid inclusion evidence for a magmatic source for metals in porphyry copper deposits: Mineralogical Association of Canada Short Course Series, v. 23, p. 139–152.

Bodnar, R.J., Burnham, C.W., and Sterner, S.M., 1985, Synthetic fluid inclusions in natural quartz: III. Determination of phase equilibrium properties in the system H_2O-NaCl at 1000°C y 1500 bars: Geochimica et Cosmochimica Acta, v. 49, p. 1861–1873.

Borisenko, A.S., 1977, Study of the salt composition of solutions in gas-liquid inclusions in minerals by the cryometric method: Soviet Geology and Geophysics, v. 18, p. 11–19.

Borrello, A.V., 1969, Los geosinclinales de la Argentina: Mendoza, Dirección Nacional de Geología y Minería, Anales XIV, Buenos Aires, p. 1–188.

Bottinga, Y., 1969, Calculated fractionation factors for carbon and hydrogen isotope exchange in the system calcite-carbon dioxide-graphite-methane-hydrogen-water vapor: Geochimica et Cosmochimica Acta, v. 33, p. 49–64.

Bouza, P., 1991, Descripción geológica y caracterización petrográfica de las vulcanitas cenozoicas aflorantes entre los arroyos Montañes y El Yeso, Cordillera Principal, Mendoza: Unpublished bachelor's dissertation, Facultad de Ciencias Exactas y Naturales, Universidad de Buenos Aires, 112 p.

Bowman, J.R., 1998, Stable-Isotope systematics of skarns: Quebec, Canada, Mineralogical Association of Canada Short Course Series, v. 26, p.99–145.

Boynton, N.V., 1989, Cosmochemistry of the rare earth elements: Condensation and evaporation processes: Reviews in Mineralogy, v. 21, 24 p.

Burnham, C.W., 1979, Magmas and hydrothermal fluids, *in* Barnes, H., ed., Geochemistry of hydrothermal ore deposits: N.Y., Wiley and Sons, p. 71–136.

Chacko, T., Riciputi L.R., Cole, D.R., and Horita, J., 1999, A new technique for determining equilibrium hydrogen isotope fractionation factors using the ion microprobe: Application to the epidote-water system: Geochimica et Cosmochimica Acta, v. 63, p. 1–10.

Chappell, B.W., and White, A. J.R., 1992, I- and S-type granites in the Lachland fold belt: Transactions of the Royal Society of Edinburgh, v. 83, p. 1–26.

Crawford, M.L., 1981, Phase equilibria in aqueous fluid inclusions: Mineralogical Association of Canada Short Course Series Handbook, v. 6, p. 75–100.

Cline, J.S., and Bodnar, R.J., 1991, Can economic porphyry copper mineralization be generated by a typical cal-alkaline melt?: Journal of Geophysical Research, v. 96, p. 8113–8126.

——1994, Direct evolution of brine from crystallizing silicic melt at the Questa, New Mexico, molybdenum deposit: Economic Geology, v. 89, p. 1780–1802.

Cole, D.R., Horita, J., Eniamin, V., Polyakov, V.B., Valley, J.W., Spicuzza, M.J., and Coffey, D.W., 2004, An experimental and theoretical determination of oxygen isotope fractionation in the system magnetite-H_2O from 300 to 800°C: Geochimica et Cosmochimica Acta, v. 68, p. 3569–3585.

Davidson, J.P., Fergusson, K.M., Colucci, M.T., and Dungan, M.A., 1988, The origin and evolution of magmas from the San Pedro-Pellado volcanic complex, S. Chile: Multicomponent sources and open system evolution: Contributions to Mineralogy and Petrology, 100, p. 429–445.

Dessanti, R.N., 1978, Descripción de la Hoja 28b, Malargüe, Pcia. de Mendoza: Boletín Servicio Geológico Nacional (Argentina), Buenos Aires, 149, p. 1–50 (and 1 map with 2 cross sections).

Droop, G.T.R., 1987, A general equation for estimating Fe^{3+} in ferromagnesian silicates and oxides from microprobe analysis, using stoichiometric criteria: Mineral Magazine v. 51, p. 431–437.

Einaudi, M., Meinert L., and Newberry, R., 1981, Skarn deposits: Economic Geology 75th Anniversary Volume, p. 317–391.

Espinoza, S., Véliz, H., Esquivel, J., Arias, J., and Moraga, A., 1996, The cupriferous province of the Coastal Range, northern Chile: Society of Economic Geologists Special Publication Number 5, p. 19–32.

Ettlinger, A.D., 1990, A geological analysis of gold skarns and precious metal enriched iron and copper skarns in British Columbia, Canada: Unpublished Ph.D. thesis, Washington State University, 249 p.

Foster, D.B., Seccombe, P.K., and Philips, D., 2004, Controls on skarn mineralization and alteration at the Cadia deposits, New South Wales, Australia: Economic Geology, v. 99, p. 761–788.

Fournier, R.O., 1999, Hydrothermal processes related to movement of fluid from plastic into brittle rock in the magmatic-hydrothermal environment: Economic Geology, v. 94, p. 1193–1211.

Franchini, M.B., and Dawson, M., 1999, Manifestaciones metálicas asociadas a skarns del Suroeste de Mendoza y noroeste de Neuquén, *in* Zappettini, E., ed., Recursos Minerales de la República Argentina: Instituto de Geología y Recursos Minerales SEGEMAR, Buenos Aires, Anales 35, p. 1535–1545.

Franchini, M.B., Meinert, L.D., and Montenegro, T.F., 2000, Skarn related to porphyry-style mineralization at Caicayen Hill, Neuquén, Argentina: Composition and evolution of hydrothermal fluids: Economic Geology, v. 95, p. 1197–1213.

Franchini, M.B., López Escobar, L., Schalamuk, I.B.A., and Meinert, L., 2003, Magmatic characteristics of the Paleocene Cerro Nevazón region and other Late Cretaceous to Early Tertiary calc-alkaline subvolcanic to plutonic units in the Neuquén Andes, Argentina: Journal of South American Earth Sciences, v. 16, p. 399–421.

Franchini, M.B., de Barrio, R. E., Ríos, F.J., Schalamuk, I.B., Lanfranchini, M., and Pons, M.J. 2005, Geología, química mineral y paragénesis del depósito Hierro Indio, Mendoza, guías para la exploración de skarns de Fe, *in* Llambías E., de Barrio R., González P., Leal P. eds., XVI Congreso Geológico Argentino: Asociación Geológica Argentina, Actas, v. 2, p. 303–310.

Franchini, M.B., de Barrio, R., Pons, M.J., Schalamuk, I.B.A., Ríos, F.J, and Meinert, L., 2007, Fe skarns and IOCG-, and manto-type deposits in the Andes Cordillera of SW Mendoza (34-36°LS), Argentina: Exploration and Mining Geology, v. 16, p. 233–265.

Godfrey, J.D., 1962, The deuterium content of hydrous minerals from the east-central Sierra Nevada and Yosemite National Park: Geochimica et Cosmochimica Acta, v. 26, p. 1215–1245.

Graham, C.M., Sheppard, S.M.F., and Heaton, T.H.E., 1980, Experimental hydrogen isotope studies: Systematic of hydrogen isotope fractionation in the systems epidote-H_2O, zoisite-H_2O and AlO (OH)-H_2O: Geochimica et Cosmochimica Acta v. 44, p. 353–364.

Gulisano, C.A., and Gutiérrez Pleimling, A.R., 1995, Field Guide: The Jurassic of the Neuquén Basin, Mendoza Province: Asociación Geológica Argentina, serie E, no. 3, 103 p.

Hemley, J.J., and Hunt, J.P., 1992, Hydrothermal ore-forming processes in the light of studies in rock-buffered systems: II Some general geologic applications: Economic Geology, v. 87, p. 23–43.

Hemley, J.J., Cygan, G.L, Fein, J.B., Robinson, G.R., and D´Angelo, W.M., 1992, Hydrothermal ore-forming processes in the light of studies in rock-buffered systems: iron-copper-zinc-lead sulfide solubility relations: Economic Geology, v. 87, p. 1–22.

Hildreth, W.E., and Moorbath, S., 1988, Crustal contribution to arc magmatism in the Andes of Central Chile: Contributions to Mineralogy and Petrology, v. 98, p. 455–489.

Irvine, T., and Baragar, W., 1971, A guide to the chemical classification of the common volcanic rocks: Canadian Journal of Earth Sciences, v. 8, p. 523–548.

Kozlowski, E., Manceda, R., and Ramos, V., 1993, Estructura, *in* Ramos, V.A., ed., Geología y Recursos Naturales de Mendoza: Relatorio del XII Congreso Geológico Argentino y II Congreso Exploración de Hidrocarburos, 1 v. 18, p. 235–2.

Leake B. E., Woolley, A., Arps C. E. S., Birch, W. D., Gilbert, M. C., Grice, D. J., Hawthorne, C. F., Kato A., Kisch, H. J., Krivovichev, V. G., Linthout K., Laird, J., Mandarino, J. A., Maresch, W. V., Nickel, E. H., Rock N. M. S., Schumacher J. C., Smith, D. C., Stephenson, N. C. S, Ungaretti L., Whittaker, E. J. W. and Youzhi, G., 1997, Nomenclature of amphiboles: Report of Subcommittee on Amphiboles of International Mineralogical Association, Commission on New Minerals and Mineral Names. American Mineralogist, v. 82, p. 1019–1037.

Legarreta, L., Gulisano, C.A., and Uliana, M.A., 1993, Las secuencias sedimentarias Jurásico-Cretácicas, *in* Ramos, V.A., ed., Geología y Recursos Naturales de Mendoza: Relatorio del XII Congreso Geológico Argentino y II Congreso Exploración de Hidrocarburos, 1 (9), p. 87–114.

López Escobar, L., 1984, Petrology and chemistry of volcanic rocks of the southern Andes, *in* Harmon, R.S., and Barreiro, B.A., eds., Andean magmatism: Chemical and isotopic constraints: Bristol, Shiva Pub. Ltd., p. 47–71.

McCrea, J.M., 1950, On the isotopic chemistry of carbonates and a paleotemperature scale: Journal of Chemical Physics, 18, p. 849–857.

Meinert, L.D., 1984, Mineralogy and petrology of iron skarn in western British Columbia, Canada: Economic Geology, v. 79, p. 869–882.

——1995, Compositional variation of igneous rocks associated with skarn deposits—chemical evidence for a genetic connection between petrogenesis and mineralization: Mineralogical Association of Canada Short Course Series, v. 23, p. 401–418.

Meinert, L.D., Hedenquist, J.W., Satoh, H., and Matsuhisa, Y., 2003, Formation of anhydrous and hydrous skarn in Cu-Au Ore deposits by magmatic fluids: Economic Geology, v. 98, p. 147–156.

Meinert, L.D., Dipple, G., and Nicolescu, S., 2005, World skarn deposits: Economic Geology 100th Anniversary Volume, p. 299–336.

Méndez, V., Zanettini, J.C., and Zapettini, E.O., 1995, Geología y metalogénesis del orógeno Andino central, República Argentina: Anales N° 23 de la Dirección Nacional del Servicio Geológico, Secretaría de Minería de la Nación, Buenos Aires, 190 p.

Morimoto, N., Fabries, J., Ferguson, A.K., Ginzburg, I.V., Ross, M., Seifert F.A., Zussman, J., Aoki, K., and Gottardi, 1988, Nomenclature of pyroxenes: American Mineralogist, v. 73, p. 1123–1133.

Mpodozis, C. and Ramos, V.A. 1989, The Andes of Chile and Argentina, *in* Ericksen, G.E. Cañas, M.T., and Reinemud, J.A. eds., Geology of the Andes and its relation to hydrocarbon and mineral resources: Circum Pacific Council for Energy and Mineral Resources, Earth Science Series, v. 11, p. 59–90.

Nash, J.T., 1976, Fluid inclusion petrology-data from porphyry copper deposits and application to exploration. U.S. Geologyical Survey Professional Paper 907-D, 16 p.

Nullo, F.E., Stephens, G.C., Otamendi, J., and Baldauf, P.E., 2002, El volcanismo del Terciario superior del sur de Mendoza: Revista de la Asociación Geológica Argentina, v. 57 (2), p. 119–132.

Ohmoto, H., and Rye, R.O., 1979, Isotope of sulfur and carbon, *in* Barnes, H.L., ed., Geochemistry of hydrothermal ore deposits: N.Y., Wiley and Sons, p. 509–567.

Pearce, J., 1996, A user's guide to basalt discrimination diagrams: *in* Wyman, D.A., ed., Trace element geochemistry of volcanic rocks: Apliccations for massive sulphide exploration: Geological Association of Canada Short Course Notes 12, p. 79–114.

Pollard, P., 2000, Evidence of a magmatic fluid and metal source for Fe-oxide Cu-Au mineralization: *in* Porter, T.M, ed., Hydrothermal iron oxide copper-gold and related deposits: A global perspective: Adelaide, Australian Mineral Foundation, p. 27–41.

Pons, M.J., 2007, Geología y Metalogénesis del skarn de hierro Vegas Peladas, Cordillera Principal, Pcia. de Mendoza: Unpublished Ph.D. thesis, Argentina, Facultad de Ciencias Naturales y Museo, Universidad Nacional de La Plata, 308 p.

Pons, M.J., Franchini, M.B., and López Escobar, L., 2007, Los cuerpos ígneos neógenos del Cerro de Las Minas (35.3° S -69.9°O), Cordillera Principal de los Andes, SO de Mendoza: Geología, Petrografía y Geoquímica: Revista de la Asociación Geológica Argentina, v. 62, p. 267–282.

Ramos, V.A., 1999a, Las provincias geológicas del territorio Argentino, *in* Zappettini, E.O., ed., Recursos Minerales de la República Argentina: Instituto de Geología y Recursos Minerales, Servicio Geológico Minero Argentino, SEGEMAR, Anales 35, 1, p. 41–96.

——1999b, Rasgos estructurales del territorio Argentino, *in* Zappettini, E. O. ed., Recursos Minerales de la República Argentina: Instituto de Geología y Recursos Minerales, Servicio Geológico Minero Argentino, SEGEMAR, Anales 29, (24), p. 715–784.

Ramos, V.A., and Nullo, F., 1993, El Volcanismo de Arco Cenozoico, *in* Ramos V.A., ed., Geología y Recursos Naturales de Mendoza: 12° Congreso Geológico Argentino, Relatorio, 1 (19), p. 149–160.

Ramos, V.A., Cegarra, M. y Cristallini, E. 1996, Cenozoic tectonics of the High Andes of west-central Argentina (30-36º latitude): Tectonophysics v. 259 p. 185–200.

Rickwood, P.C., 1968, On recasting analyses of garnet into end-member molecules: Contribution to Mineralogy and Petrology, v. 18, p. 175–198.

Rollinson, H.R., 1993, Using geochemical data: Evaluation, presentation, interpretation: Singapore, Longman Singapore Publishers (Pte) Ltd., 352 p.

Sharp, Z.D, 1990, A laser-based microanalytical method for the in situ determination of oxygen isotope ratios of silicates and oxides: Geochimica et Cosmochimica Acta, v. 54, p. 1353–1357.

Sharp, Z.D., and Kirschner, D.L., 1994, Quartz-calcite oxygen isotope themometry: a calibration based on natural isotopic variations: Geochimica et Cosmochimica Acta, v. 58, p. 4491–4501.

Shepherd, T.J., Rankin, A.H, and Alderton, D.H.M, 1985, A practical guide to fluid inclusion studies: New York, Blackie and Son, 237 p.

Sidder, G.B., 1985, Ore genesis at the Monterrosas deposit in the Coastal batholith, Ica, Peru: Unpublished Ph.D. thesis, Oregon State University, 221 p.

Simon, A.C., Pettke, T., Philip, A.C., Philip M.P., and Henrich, C., 2004, Magnetite solubility and iron transport in magmatic-hydrothermal environments: Geochimica et Cosmochimica Acta, v. 68, p. 4905–4914.

Sterner, M.S., Hall, D.L., and Bodnar, R.J., 1988, Synthetic fluid inclusions. V. Solubility relations in the system NaCl-KCl-H_2O under vapor-saturated conditions: Geochimica et Cosmochimica Acta, v. 52, p. 989–1005.

Taylor, B.E., 1986, Magmatic volatiles: Isotopic variation of C, H, and S: Reviews in Mineralogy, v. 16, p. 185–226.

Tormey, R.D., Frey, F.A., and López Escobar, L., 1991, Recent lavas from the Andean volcanic front (33 to 42° S); Interpretations of along-arc compositional variations: Geological Society of America Special Paper 265, p. 57–77.

Uliana, M.A., Biddle, K.T., and Cerdan J., 1989, Mesozoic extension and the formation of Argentine sedimentary basins: Tulsa, American Association of Petroleum Geologists, Memoir, 46, p. 599–614.

Vicente, J.C., 1975, Essai d'organiztion paleogeographique et estructurale du paleozoique des Andes Méridionales: Geologische Rundschau v. 64, p. 343–394.

Whitney, J.A, Hemley J.J., and Simon F.O., 1985, The concentration of iron in chloride solutions equilibrated with synthetic granitic compositions: The sulfur-free system: Economic Geology, v. 80, p. 444–460.

Williams, P.J., 1999, Fe-oxide-Cu-Au deposits of the Olympic Dam/Ernest Henry-type, In New developments in the understanding of some major ore types and environments, with implications for exploration: Toronto, Prospectors and Developers Association of Canada Short Course, p. 1–43.

Yang, K., and Bodnar, R.J., 1994, Magmatic-hydrothermal evolution in the "Bottoms" of porphyry copper systems: Evidence from silicate melt and aqueous fluid inclusions in granitoid intrusions in the Gyeongsang basin, South Korea: International Geology Review, v. 36, p. 608–628.

Yrigoyen, M.R., 1979, Cordillera Principal, *in* Turner J.C.M., ed., II Simposio de Geología Regional Argentina: Córdoba, Academia Nacional de Ciencias, Proceedings, v. 1, p. 651–694.

Zhang, Y.G., and Frantz, J.D., 1987, Determination of homogenization temperatures and densities of supercritical fluids in the system NaCl-KCl-$CaCl_2$-H_2O using synthetic fluid inclusions: Chemical Geology, v. 64, 335–350.

Zhao, Y., Lin, W., Bi, C., and Li, D., 1990, Skarn deposits in China: China, Beijing Geological Publishing House, 354 p.

Zheng, Y.F., 1991, Calculation of oxygen isotope fractionation in metal oxides: Geochemica et Cosmochimica Acta, v. 55, p. 2299–2307.

——1993a, Calculation of oxygen isotope fractionation in anhydrous silicate minerals: Geochimica et Cosmochima Acta v. 57, p. 1079–1091.

——1993b, Calculation of oxygen isotope fractionation in hydroxyl-bearing silicates: Earth and Planetary Science Letters, v. 120, p. 247–263.

——1999, Oxygen isotope fractionation in carbonate and sulfate minerals: Geochemical Journal, v. 33, p. 109–126.

Zheng, Y.F., and Simon, K., 1991, Oxygen isotope fractionation in hematite and magnetite: A theoretical calculation and application to geothermometry of metamorphic iron-formation: European Journal of Mineralogy, v. 3, p. 877–886.

Zürcher, L., Ruíz, J., and Barton, M., 2001, Paragenesis, elemental distribution, and stable isotopes at the Peña Colorada iron skarn, Colima, Mexico: Economic Geology, v. 96, p. 535–557.